Chapter 2
Nuclear Energy and Its Role in Hydrogen Production

Abstract In this chapter the role of nuclear energy in hydrogen production at large scale is discussed. In the first part of the chapter various routes of hydrogen generation using nuclear energy are described. Five routes are identified for hydrogen generation by water splitting, among which four are based on thermal energy derived from nuclear reactor, while the fifth is based on the radiolytic effect (that is, disintegration of water molecule under the impact of nuclear radiation). The role of hydrogen as energy storage medium for load levelling of the regional electrical grid is extensively discussed. It is shown that hydrogen production when electricity demand is low, storage and its use in fuel cell for power generation when electricity demand is high, represents a very attractive method for effective generation of electricity in regional grids, which reduces the costs and decreases the environmental production when nuclear energy is the primary source. Large-scale hydrogen production is also essential for petrochemical operations and heavy (nonconventional) oil upgrading, or oil-sand extraction/processing procedures. Hydrogen option represents a potential solution for transportation sector where it can be used either directly (hydrogen is stored onboard of vehicles) or indirectly (hydrogen is converted in a synthetic fuel such as gasoline, diesel, methanol, or ammonia). All means of transportation can benefit from hydrogen as energy carrier; in this chapter the road, rail, and air transport are analyzed in detail.

2.1 Introduction

The constant rise of energy demand in the world imposes an increasing supply of power generation capacity, while efforts must be made to reduce the greenhouse gas (GHG) emissions associated with higher capacity. In addition to clean electricity generation, there is a need for high-temperature thermal energy supply by methods with reduced pollution. As a result, worldwide research efforts are focusing on the development of renewable energy technologies, such as wind, concentrated solar thermal, ocean, biomass, geothermal, among others.

G.F. Naterer et al., *Hydrogen Production from Nuclear Energy*,
DOI 10.1007/978-1-4471-4938-5_2,

Although the generation potential from renewable sources is sufficient to satisfy the energy needs of humankind, their relatively high costs have limited their large-scale adoption. A major challenge with solar energy is its day–night intermittency and intensity fluctuation. Solar-to-hydrogen technology can reach an efficiency of a few percent at an elevated cost. Wind power fluctuates and it is characterized by a small capacity factor. Massive use of biomass energy has ethical issues related to the dilemma of "crops for energy or crops for food." Exploitable geothermal sources are limited.

In the energy mix of the future, there is a need for a stable source of energy that can assure a base load without GHG emissions. For this goal, nuclear energy must be considered. All nuclear power stations presently in operation are designed to steadily generate electricity to satisfy the base load of an electrical grid. There are an increasing number of countries that are adopting nuclear energy programs, showing a growing worldwide effort to develop a fourth generation of nuclear reactors for combined power, high-temperature heat, and hydrogen. In the future, all energy systems are expected to be hybrid systems, which are a combination of various energy resources and energy conversion methods to operate as one system, to maximize efficiency and to reduce environmental impact and waste heat. Hydrogen is a promising energy carrier to link between renewable and nuclear energy sources in those hybrid systems which are sustainable and environmentally benign. A non-exhaustive list of advantages of nuclear hydrogen production is given as follows.

- It generates a new market—hydrogen—which can be sold either as electricity (via fuel cells) during peak periods when the price is higher, or as fuel for transportation, or as a chemical feedstock to industry, whichever is more advantageous.
- It levels the electricity demand profile of the grid.
- It allows for more efficient power production as the generators (other than nuclear) can operate mostly near to their nominal load.
- It reduces pollution associated with power production because the generators operate with higher efficiency.
- It aids development of renewable energy sources which need temporary energy storage (such as hydrogen) to smooth the fluctuating availability profile.
- It makes nuclear power plants more cost competitive and secure by integration with high-temperature electrolysis and thermochemical cycles.

In this chapter, the role of nuclear energy for hydrogen production is discussed and related issues are analyzed. The objective is to introduce the main methods of hydrogen production from nuclear energy and to study three major roles of nuclear hydrogen, namely: (1) energy storage medium for load levelling of an electrical grid, (2) promoting cleaner petrochemical operations, and (3) providing an environmentally benign fuel for the transportation sector.

2.2 Nuclear Hydrogen Production

Nuclear energy is generated in fission reactors using uranium-based fuel (or thorium in the near future). The generated nuclear radiation is converted to high-temperature heat which is transported by a heat transfer fluid for further use. The regular use of nuclear heat is power generation in large-scale power plants. It is possible to divert some of the high-temperature heat from nuclear reactors to supply chemical processes that eventually generate hydrogen from water splitting. Moreover, nuclear radiation present in nuclear reactors and during all phases of nuclear fuel processing can be used directly to generate hydrogen from water.

Five general methods can be envisaged to generate hydrogen from nuclear energy through water decomposition: (1) radiolysis, (2) electrolysis, (3) high-temperature steam electrolysis, (4) hybrid thermochemical water splitting, and (5) thermochemical water splitting. Method (1) uses nuclear radiation to directly split the molecule of water into hydrogen and oxygen; method (2) uses electricity derived from nuclear energy to electrolyze water; methods (3) and (4) are called hybrid because they use both electricity and high-temperature heat to split water; and method (5) directly uses high-temperature heat. All possible paths of water splitting using nuclear energy are represented in Fig. 2.1. As shown in the figure, nuclear energy is converted into nuclear radiation (either in the reactor or during the fuel processing cycle). Nuclear radiation is converted further to high-temperature heat. Both the radiation and heat are used to generate hydrogen, as indicated.

The radiolytic (also known as chemo-nuclear) water splitting method uses high-energy radiation or kinetic energy of fission products to excite water molecules and generate hydrogen and oxygen. Experiments of Carty et al. (1981) show that water can be split with fission fragments and steam can be split by alpha particle irradiation. An experiment of alpha irradiation of steam splits six water molecules with 100 eV radiation, which corresponds to 15 % efficiency (Carty et al. 1981). However, with current commercial reactors, a configuration for radiolytic water splitting is not practical because of requirements of containment of the radioactive material, although radiolysis can, in principle, be implemented at spent fuel pools of existing nuclear power plants.

The alternative option is to use high-temperature heat in four ways mentioned above (2–5). In current nuclear reactors, nuclear particles are thermalized (slowed by collisions) and nuclear radiation is transferred with the purpose to convert nuclear energy into heat. A thermal fluid is used to carry the heat from the confined nuclear reactor. Using this heat to split water implies a requirement to supply the required Gibbs energy and enthalpy to each molecule.

Figure 2.2 shows the variation of Gibbs free energy and enthalpy of water dissociation with temperature. The Gibbs energy for water dissociation can be calculated from the reaction enthalpy and entropy of $H_2O(l) \rightarrow H_2(g) + 0.5O_2(g)$ with the equation $\Delta G = \Delta H - T \times \Delta S$, where T is the temperature at which the reaction occurs.

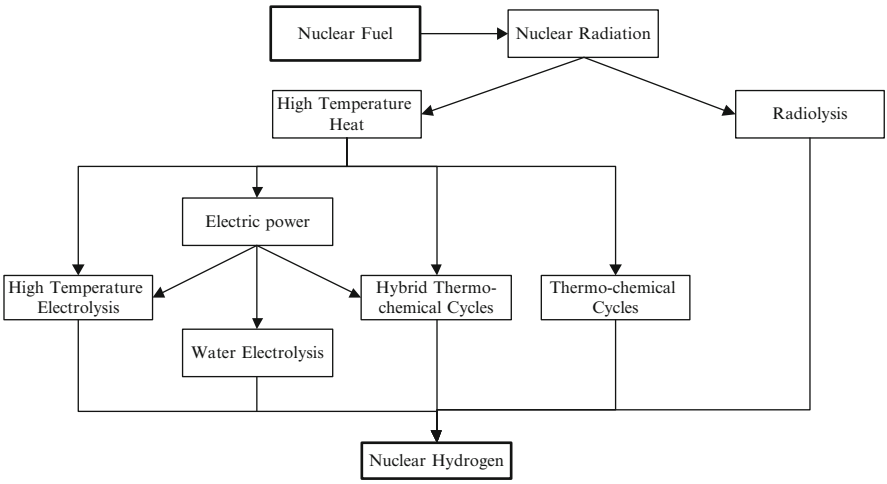

Fig. 2.1 Nuclear water splitting pathways for hydrogen production

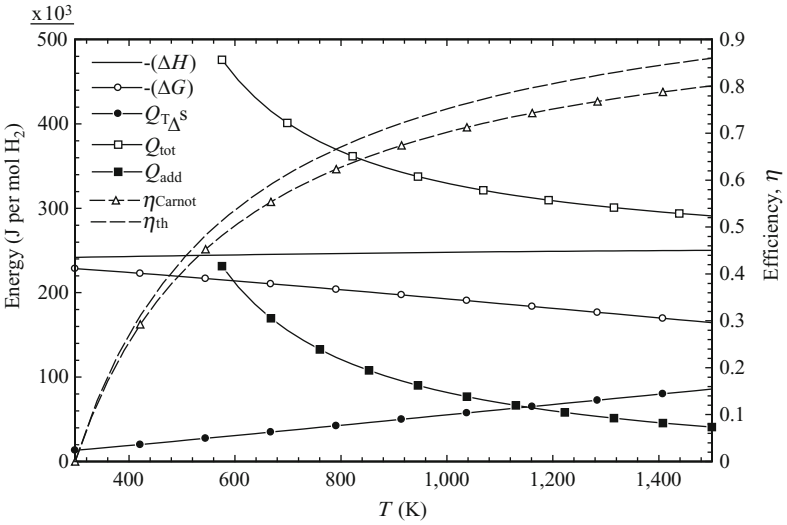

Fig. 2.2 Thermal energy to split 1 mol of water molecule and its required conversions

Although the reaction enthalpy increases with temperature, the Gibbs energy decreases. The Gibbs energy cannot be transferred as heat; it requires an organized form of energy such as work, electricity, high-energy radiation, etc. Method (2) mentioned above uses electricity only to split water molecules by electrolysis. A part of the electrical energy supplied at the electrodes is received by the molecules of water as the Gibbs free energy. The other part, $Q_{T\Delta S} = -T \times \Delta S$, is transmitted as heat, although it is provided in electrical form at the electrodes of the

electrolyzer. The $Q_{T\Delta S}$ term originates from internal conversion of electricity into heat, by Joule effects within the electrolyte. The total energy supplied fully electrically to the electrolyzer is therefore $\Delta H = \Delta G + Q_{T\Delta S}$. It can be observed from Fig. 2.2 that the ratio between ΔG and ΔH decreases with temperature. At 298 K, ΔG is 98 % of ΔH; at 1,500 K, this ratio reaches 66 %. This suggests that water electrolysis (method 2) is applicable at temperatures close to the standard value. However, at higher temperatures, other hybrid electrothermal methods (3, 4) or thermal-only methods (5) are applicable.

The energy delivered by the future generation of nuclear reactors will be in the form of high-temperature heat. The level of temperature will be increased with respect to reactors today. For example, the planned CANDU-SWCR reactor generates heat at 650 °C, as compared with the present CANDU-6 which delivers steam at 330 °C. For a water splitting reaction that is conducted at a given temperature T, the heat needed to supply the required Gibbs energy to the reaction can be calculated from the following equation:

$$\Delta G = Q_{\Delta G} \times (1 - T_0/T), \tag{2.1}$$

where T_0 is the reference temperature of the environment. The amount of heat required to drive the water splitting reaction becomes $Q_{\text{tot}} = Q_{\Delta G} + Q_{T\Delta S}$. The heat flow $Q_{\text{add}} = Q_{\text{tot}} - |\Delta H|$ is the minimum additional heat that must be available over the heat corresponding to water dissociation in order to be able to deliver to the molecules the required Gibbs energy and the energy necessary to compensate for the irreversibilities $(-T\Delta S)$. Figure 2.2 indicates the variation of Q_{tot} and Q_{add} with reaction temperature. The maximum thermal efficiency of the water splitting process can be determined by

$$\eta_{\text{th}} = \frac{\Delta H}{Q_{\text{tot}}}. \tag{2.2}$$

According to Fig. 2.2, the maximum thermal efficiency at 825 K (maximum temperature within the Cu-Cl water splitting cycle) is 0.68, and at 1,500 K (viz. high-temperature steam electrolysis) is 0.86. For these temperatures, the Carnot efficiency is 0.64 and 0.80, respectively. The Carnot efficiency curve is also indicated in Fig. 2.2. From this analysis, it is thermodynamically advantageous to generate hydrogen from high-temperature sources because a certain amount of transferred heat (namely, $Q_{T\Delta S}$) can be used directly as thermal energy for the process. This shows the advantage of nuclear hydrogen production by hybrid or thermal-only methods.

The production of hydrogen by water electrolysis does not require the electrolyzer to be placed at the nuclear plant site. It is possible to use distributed electrolyzers connected to the electrical grid. This method is beneficial for the entire grid, including the nuclear power generator, because it allows for load levelling. Section 2.3 of this chapter discussed the importance of delocalized

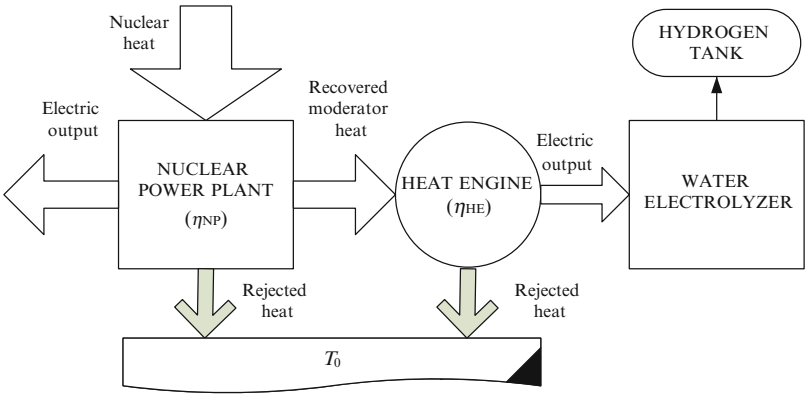

Fig. 2.3 Cogeneration of hydrogen at nuclear power plants from recovered moderator heat

water electrolysis in synergy with thermochemical production at a nuclear power plant site. Another method for nuclear-based water electrolysis is indicated in Fig. 2.3; it couples the moderator to a heat engine which produces more power to operate an electrolyzer. Water electrolyzers, discussed in Chap. 4, have a practical electricity-to-hydrogen efficiency of about $\eta_E = 60\,\%$. Nuclear reactors of the present generation have an efficiency of typically $\eta_{NP} \cong 30\,\%$. The efficiency is over 45 % with a fourth-generation modular helium reactor (MHR) and advanced gas reactor (AGR). If heat rejected by moderator of nuclear power plant is recovered and used to drive a heat engine, then power generation efficiency limited by a Carnot factor of the order of 12 %, thus an achievable $\eta_{HE} = 6\,\%$. It results in a practical recovered heat-to-hydrogen efficiency of $6\,\% \times 60\,\% = 3.6\,\%$. With the assumption that moderator heat represents 5 % of the heat rejected by a power plant, it results in generated hydrogen that represents an equivalent energy of maximum 1 % from the generated power. At a scale of production of 700 MW, the hydrogen production would be significant, approximately 600 kg/day.

The thermal-to-hydrogen efficiency of high-temperature electrolyzers, hybrid and direct thermochemical water splitting cycles is limited as indicated by the η_{th} curve in Fig. 2.2. High-temperature steam electrolyzers operate at ~1,000 °C. The electricity-to-hydrogen efficiency can be over 90 %, as discussed in Chap. 5. With a 30 % efficiency of power generation, it results in 27 % nuclear heat-to-hydrogen efficiency. In high-temperature electrolysis, at least a portion of energy equal to the Gibbs energy of the reaction must be given as electricity. If a hybrid thermochemical cycle is used instead, the required electricity is typically much smaller than the Gibbs energy for water splitting at that temperature. On the other hand, the heat requirement is higher than $Q_{T\Delta S}$. Direct thermochemical cycles do not require electrical energy input. In Fig. 2.4 the layout of a system for coupling nuclear reactor with thermal of hybrid water splitting systems is suggested. A part of the heat from nuclear reactor and a part of the power generated by the nuclear power plant are supplied to water splitting system.

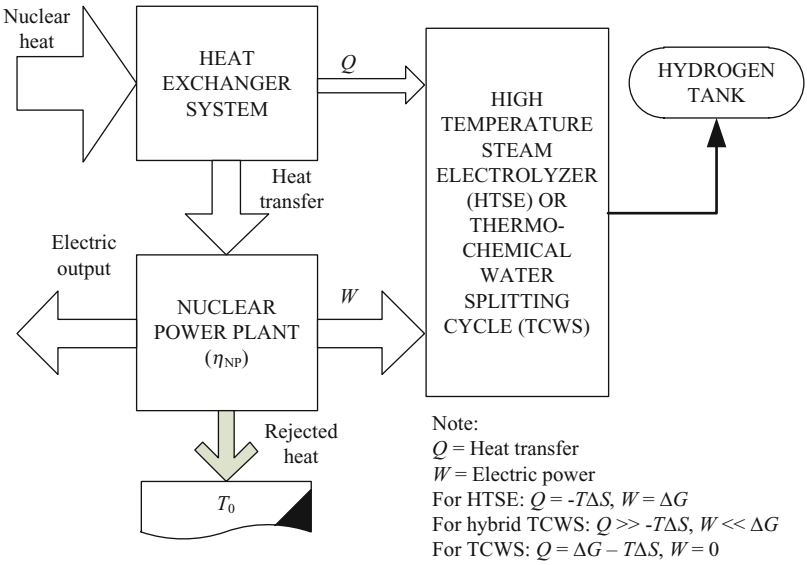

Fig. 2.4 Configuration for coupling high-temperature steam electrolysis or thermochemical water splitting cycle with a nuclear reactor

In the following sections, thermochemical cycles that can be adapted to nuclear reactors of the fourth generation are described. Thermochemical cycles aim to reduce the amount of electricity and the temperature for water splitting reactions via a number of intermediate steps in which additional chemical reactions occur. The overall reaction is $H_2O \rightarrow H_2 + 0.5O_2$. In a multistep process it is, in theory, possible to decrease the work requirement to as low as zero by performing reactions with positive entropy changes at high temperatures and reactions with negative entropy changes at low temperatures.

The sulfur–iodine cycle (S–I) comprises three steps and requires heat input at 800–1,000 °C. The first step is the Bunsen reaction according to $I_2 + SO_2 + 2H_2O \rightarrow 2HI + H_2SO_4$ in which exothermic sulfur dioxide (SO_2) gas absorption takes place in the liquid phase at 20–100 °C. Gaseous SO_2 reacts with iodine (I_2) and water (H_2O) to generate an aqueous solution of hydriodic acid (HI) and sulfuric acid (H_2SO_4). Then the two types of acids produced at the end of the reaction are separated by liquid–liquid-phase separation in the presence of excess iodine. The HI decomposition reaction $2HI \rightarrow I_2 + H_2$ generates hydrogen with a low endothermic heat of reaction at 300–500 °C in the gas phase. The H_2SO_4 decomposition reaction occurs according to $H_2SO_4 \rightarrow H_2O + SO_2 + 0.5O_2$ in two stages; at first, gaseous H_2SO_4 decomposes into H_2O and SO_3 at 400–500 °C; secondly, SO_3 decomposes into SO_2 and O_2 at about 800 °C with the help of a solid catalyst. The sulfur–iodine cycle is discussed in detail in Chap. 6.

A variation of the S–I cycle is the sulfuric acid cycle developed initially by the Japan Atomic Energy Agency (JAEA). It includes a low-temperature electrolytic process at 450 °C of sulfuric acid decomposition, $H_2SO_4 \rightarrow H_2O + SO_3$, using a solid electrolyte that conducts oxygen ions. The sulfur trioxide is decomposed thermally, $SO_3 \rightarrow SO_2 + 0.5O_2$ at 550 °C, and the sulfur dioxide is combined electrochemically with water at 80 °C to release hydrogen according to $2H_2O + SO_2 \rightarrow H_2SO_4 + H_2$.

The ISPRA Mark 9 thermochemical cycle requires 650 °C as a maximum temperature to drive a hydrolysis reaction of iron dichloride according to $6FeCl_2 + 8H_2O \rightarrow 2Fe_3O_4 + 12HCl + 2H_2$. It follows a chlorination step of magnetite occurring at 150 °C, and a decomposition step of iron tri-chloride $6FeCl_3 \rightarrow 3Cl_2 + 6FeCl_2$ conducted at 430 °C.

The lithium-nitrite cycle proposed by the Argonne National Laboratory (ANL) comprises three steps, namely, (1) hydrogen iodide production, $LiNO_2 + I_2 + H_2O \rightarrow LiNO_3 + 2HI$ by oxidation of lithium nitrite at about 25 °C; (2) hydrogen production through thermal decomposition of hydrogen iodide, $2HI \rightarrow H_2 + I_2$ at 425 °C; and (3) lithium nitrate decomposition, $LiNO_3 \rightarrow LiNO_2 + 0.5O_2$ at 475 °C.

The magnesium-chloride cycle was studied at ANL and the Idaho National Laboratory. It comprises three steps, one of which is the electrolysis of anhydrous hydrochloric acid, $2HCl \rightarrow H_2 + Cl_2$. The second step occurs as chlorination of magnesium oxide, $MgO + Cl_2 \rightarrow MgCl_2 + 0.5O_2$ at 500 °C, while the third step is the hydrolysis of magnesium chloride, $MgCl_2 + H_2O \rightarrow 2HCl + MgO$ at 450 °C.

Atomic Energy of Canada Limited (AECL) and ANL have been developing a low-temperature thermochemical cycle called the copper–chlorine (Cu–Cl) cycle, which is currently under development and scale-up at the University of Ontario Institute of Technology (UOIT). It has a number of versions depending on the number of steps: three, four, and five steps. The maximum temperature required with the five-step cycle is 530 °C, which occurs as follows:

- Steam at 400 °C and solid copper chloride ($CuCl_2$) at 400 °C enter a fluidized bed reactor, where an endothermic chemical reaction occurs, $2CuCl_2(s) + H_2O(g) \rightarrow CuO{\cdot}CuCl_2(s) + 2HCl(g)$.
- Copper oxychloride decomposes thermally at 500 °C and releases oxygen according to the reaction $CuO{\cdot}CuCl_2(s) \rightarrow 2CuCl(l) + 0.5O_2(g)$.
- Electrolytic copper is produced, $4CuCl(s) \rightarrow 2CuCl_2(aq) + 2Cu(s)$ at 80 °C in an aqueous solution.
- The aqueous $CuCl_2$ is dried, $CuCl_2(aq) \rightarrow CuCl_2(s)$.
- Solid copper is combined with hydrochloric acid at 400 °C to produce hydrogen according to $2Cu(s) + 2HCl(g) \rightarrow 2CuCl(l) + H_2(g)$.

Orhan (2011) found through ASPEN simulations that the Cu–Cl cycle reaches a heat-to-hydrogen efficiency of over 40 %. This cycle is analyzed in detail in Chap. 7, including its variations with regard to the number of steps. Because of its required temperature level of 530 °C, the Cu–Cl cycle is the most promising cycle to be linked with the Generation IV CANDU-SWCR reactor.

2.3 Energy Storage for Load Levelling

In any market, the price is determined based on the economics of supply and demand. In the free electrical energy market, the price is determined by supply, demand, and regulation. The market comprises at least four entities: the electricity generators, the grid, the consumers, and the regulatory body. The electricity generators represent a multitude of power plants (nuclear, hydro, coal, natural gas, etc.), which supply electricity to the grid; this is called the "supply side" of the energy system. The consumers of electricity are those who determine the electricity demand (or the grid load) at any particular moment; they are denoted generically as the "demand side." The grid has a role to transport the electricity from producers to consumers. Additionally, the grid is connected to electricity storage systems able to smooth short-term fluctuations in the demand. The grid is also connected to grids of neighboring jurisdictions to allow for electricity trade by exports and imports. The regulatory body establishes the rules of economic transactions for electricity; thus it influences the market price.

There is a potential to reduce the price of electricity generated by the grid system if nuclear power plants are coupled with hydrogen production facilities. In this section, the importance of energy storage in the form of hydrogen for levelling the grid load is discussed. Moreover, the synergy between centralized base load hydrogen generation at nuclear stations and off-peak hydrogen generation by electrolysis at decentralized locations is discussed with respect to grid economics and ecological factors.

Figure 2.5 illustrates—as a typical case—the supply and demand profile for mid-July 2011 in Ontario. From these curves, the supply meets the demand only incidentally. The supply is generally higher than the demand, except for short periods when there is more demand than supply, indicating that electricity imports from neighboring provinces may be required. The normalization in Fig. 2.5 is made with respect to peak generation for the day. The grid is supplied by a mix of electrical energy generators: nuclear power stations; coal and natural power plants; and hydro, wind, solar, and other generators. Nuclear power plants operate steadily at their optimum to generate the grid base load, while other generators operate at part load.

The load factor, defined as the ratio of generated power vs. the production capability of the generator, quantifies the degree of part load. Figure 2.6 illustrates the load factor of Ontario's grid generators for mid-July 2011. Similar profiles exist for other national/regional grid systems. The nuclear power load factor is quasi-constant and around 0.98. For the coal power plants, it varies from close to 0 to 0.75; for natural gas it varies from about 0.20 to 0.60; for hydropower it starts from 0.40 in the mornings, and reaches 0.60 in the evenings and 0.05 in the night; solar power is only available during the day and it reaches its maximum load factor at about noon. Operation at part load of any power plant cannot be optimal. Therefore, any load variation can lead to efficiency losses; more fuel is needed to generate a unit of electrical energy. This is reflected in the electricity price fluctuations.

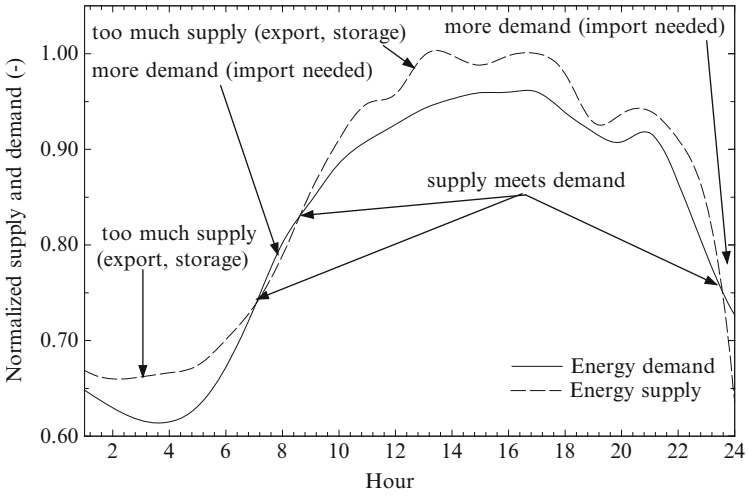

Fig. 2.5 Daily supply/demand profiles in mid-July 2011 in Ontario, Canada [data from IESO (2011)]

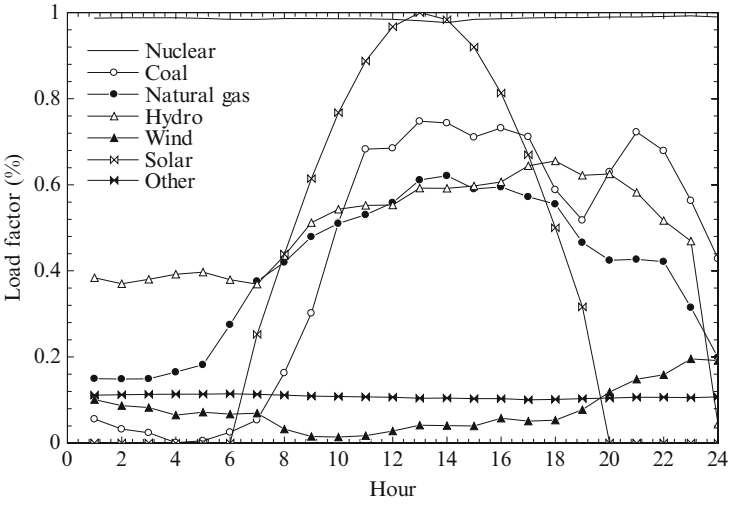

Fig. 2.6 Load factors of grid power generators by type for mid-July in Ontario [data from IESO (2011)]

In the electricity market, there is always a difference between the generated power and the generation capacity of the suppliers. The capacity is larger than the generation. The electricity price is directly influenced by the difference between the generation capability of the electrical energy system and the demand.

The pricing mechanism of electricity is further explained using actual data from an electrical grid. Figure 2.7 shows the demand and generation capability profiles of

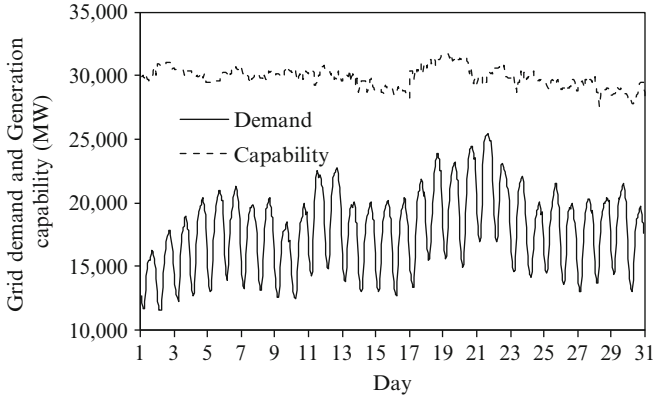

Fig. 2.7 Ontario's grid demand and generation capability in July 2011 [data from IESO (2011)]

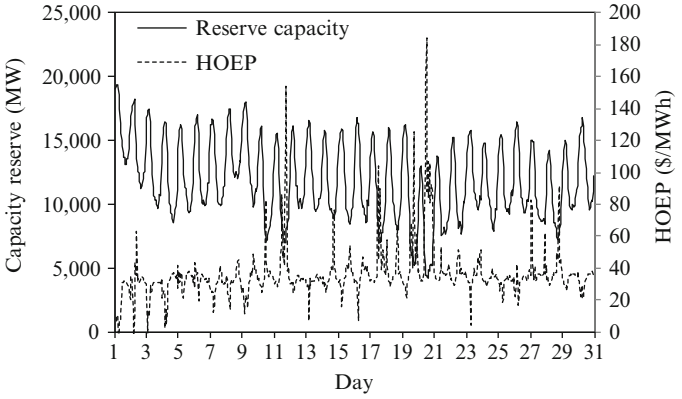

Fig. 2.8 Electricity price correlated with the reserve capacity of Ontario grid in July 2011 [data from IESO (2011); *HOEP* hourly ontario electricity price)]

Ontario's grid in July 2011. The difference between generation capability and the demand is called the "reserve capacity" of the generators. The reserve capacity of the day can be determined by subtracting the "demand" profile from the "capacity" profile. Figure 2.8 correlates the reserve capacity of generators with the hourly electricity cost. Prices are generally higher when the reserve capacity is lower. In addition, the electricity price tends to be higher at peak demand, which typically falls in early evenings when people arrive from work. In off-peak (low demand) hours (e.g., nights) and days (e.g., weekends), the electricity price is low. The low price of electricity in off-peak periods creates the opportunity to generate relatively cheap hydrogen.

The cost of grid-produced hydrogen correlates with three factors: (1) the price of electricity; (2) additional electrolysis capacity, above a continuous level that does not vary with electricity prices throughout the day; and (3) the required storage of

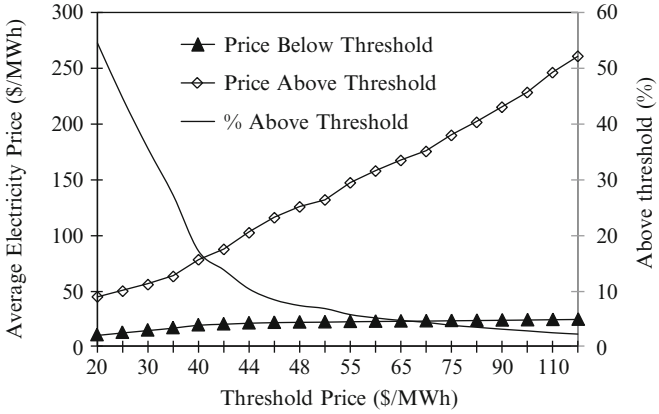

Fig. 2.9 Electricity prices above and below a threshold in Alberta, 2002

hydrogen. Note that the percentage of electricity supply above the price threshold of electricity decreases when the electricity price rises (see Fig. 2.9). If off-peak electricity is used to generate hydrogen by electrolysis, then a threshold price is established, wherein hydrogen is only produced below the threshold. When this threshold price is lowered, more capacity of electrolysis is needed to produce a given quantity of hydrogen over a shorter duration. Also, more storage capacity is needed due to longer periods without generation of hydrogen. Therefore centralized hydrogen generation should be applied.

Generation of hydrogen during the off-peak hours has many advantages. Ideally, for the best economics, the entire difference between the generation capacity and grid demand can be converted to hydrogen, as an energy carrier and storage medium. The grid can generate hydrogen in a delocalized or localized manner. Grid-connected water electrolyzers of capacity up to hundreds of kW or 1 MW can be distributed over a territory—especially in urban regions—to generate hydrogen in a delocalized manner. High-temperature electrolysis systems and thermochemical water splitting cycles can be coupled to heat-rejecting power plants to generate large quantities of hydrogen at their locations. The plants can be equipped with fuel cells to generate back electricity when the grid needs it, or the hydrogen can be sold to local transportation or industrial sectors.

In the subsequent part of this section, the additional benefits of integrating electrolysis and thermochemical hydrogen production are examined. Their unique synergy of coupling decentralized off-peak electrolysis with centralized base load thermochemical production is a significant advantage. The results are derived from work of Naterer et al. (2008). Four cases are analyzed here for hydrogen production.

- System I (benchmark): Decentralized production of hydrogen by water electrolysis.
- System II: Hydrogen production by steam-methane reforming (SMR).

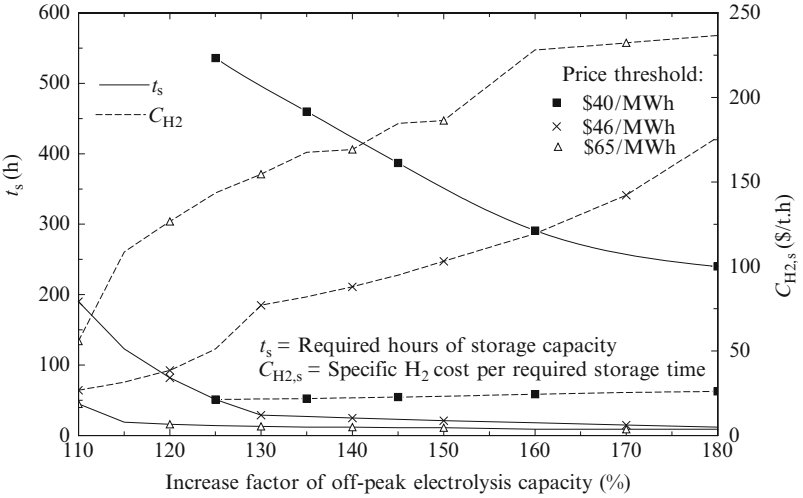

Fig. 2.10 Required hours of hydrogen storage capacity and the specific cost of hydrogen correlated to the increase factor of off-peak electrolysis capacity

- System III: Thermochemical Cu–Cl cycle (TCCC) coupled to an SWCR nuclear reactor.
- System IV: TCCC coupled to a CANDU-III reactor assisted by natural gas combustion.

For System I (the benchmark case), a capital cost of the electrolyzer of $300/kW is assumed with 15 %/year return on investment and a 10-year amortization period. The electrolysis hydrogen is stored in tubes with an assumed storage cost of $0.8M/t.

The capacity and storage of hydrogen rise when the price threshold is reduced. For a given electrolysis capacity, if the units operate only when electricity prices are the lowest, then the electrolysis units remain idle for a longer period of time, thereby increasing the required hours of storage. More storage is needed to meet demand, which increases the overall cost.

The electrolyzers are never shut down: during the off-peak hours, the electrolyzers run to a capacity much higher than that corresponding to peak hours of operation. Figure 2.10 shows the influence of the increase factor of off-peak electrolysis capacity with respect to the peak period on the storage time and specific hydrogen cost. If the off-peak capacity factor is higher, then the required hours of hydrogen storage time are reduced. The cost of hydrogen tonnage follows the same trend; however, the cost per unit mass of hydrogen per hour of storage time increases with the capacity factor of the electrolyzer for off-peak periods. Consequently, this factor must be established based on a trade-off analysis that considers the specific storage time and the costs. Moreover, one notes from Fig. 2.10 that the chosen price threshold that defines on- and off-peak periods is a parameter that influences the analysis to a large extent. An optimum exists at a particular

electrolysis installation capacity, above which the price per kg of hydrogen produced becomes excessive.

System II comprises a number of centralized plants of large capacity that generate hydrogen by SMR. Consider a capacity of SMR plant of 10 t hydrogen/day (1,420 GJ/day) which was found a suitable choice for integration with Ontario's grid. The capital cost of the SMR plant is approximated by scaling laws according to

$$C_{\mathrm{SMR}}/(\dot{m}_{\mathrm{H_2}})^{0.66} = C_{\mathrm{ref}}/(\dot{m}_{\mathrm{ref}})^{0.66}, \tag{2.3}$$

where $\dot{m}$ is the rate of hydrogen production per day and it represents the plant scale; C is the capital cost; the subscript "ref" indicates a reference case; and the exponent 0.66 is a typical scale factor for chemical plants.

For reference values in (2.3), one notes that an SMR plant of 230 t/day has a capital cost of $65M. Thus for 10 t/day, it results in $8M investment. The storage facility for hydrogen at a centralized location comprises large-size pressurized reservoirs. The associated investment cost for those is taken to be a typical value of $0.2M/t (which is lower than tube storage used for System I). The resulting SMR capital cost is $3.1/GJ, assuming a 20 % annual capital charge. If one assumes that hydrogen is transported from the centralized production facility to distributed users by trucks, there is about $0.8M additional capital reflected in truck operations; consequently the total capital in the System II capital cost is $3.9/GJ.

The operational cost of System II depends on the fluctuating price of natural gas. In addition, one has to account for natural gas distribution charges and the SMR conversion efficiency (about 79 %). With such assumptions, the estimated hydrogen price—as indicated in Naterer et al. (2008)—becomes $8.4/GJ. The cost associated to carbon dioxide sequestration is around $1.6/GJ.

System III uses the Cu–Cl cycle to split water into hydrogen and oxygen through intermediate copper and chlorine compounds. This cycle comprises a set of chemical reactions that form a closed internal loop that recycles all chemicals on a continuous basis, without emitting any GHGs externally to the atmosphere. The same (2.3) is used to determine the capital cost of a 10 t/day Cu–Cl plant. In this case, the reference values taken from a study by the Argonne National Laboratory—as cited in Naterer et al. (2008)—are $124 M for a Cu–Cl plant that produces 125 t/day of hydrogen. Accounting to capital discharge and a 3 % inflation rate up to 2015 when the cycle is assumed to become a commercial technology, it yields a contribution of $7.7/GJ for the capital portion of the hydrogen cost.

A thorough analysis with Aspen Plus software shows that a heat-to-hydrogen efficiency of the Cu–Cl cycle of 54 % is theoretically possible, as compared to 30 % which is the nuclear-to-hydrogen efficiency obtained with Canada's next generation of reactors coupled to electrolysis. Thus there is a significant margin of superior overall conversion efficiency in favor of the Cu–Cl technology. To be conservative and more realistic in the estimates, it is assumed that the heat-to-hydrogen efficiency of the Cu–Cl cycle is 43 %. This cycle allows for a high degree of heat

recovery and internal heat recycling between hotter and colder streams, thereby leaving a relatively smaller portion of between 20 and 30 % for the remaining high-temperature heat source at about 530 °C; this heat amounts to about 66 GJ/t of hydrogen. Canada's supercritical water reactor of Generation IV is designed to supply steam at 25 MPa and 625 °C, which is sufficient to supply the required heat to a Cu–Cl plant. It is assumed that a Cu–Cl plant is coupled with a medium-size nuclear reactor of 700 MW. Sample calculations show that for 10 t of hydrogen per day produced with 43 % efficiency, the amount of thermal power needed is ~40 MW, which represents 6 % of the nuclear plant capacity. There are required inputs of about 4.2 kg/s of water and 7.6 MW of heat assuming that the plant operates steadily. It results in 1 % of steam that must be extracted from the power plant and that the high-pressure working fluid (steam) can be cooled from 625 to 618 °C to deliver heat through a heat exchanger to the Cu–Cl cycle. The margin of efficiency improvement is more than one-third higher than the overall heat-to-hydrogen efficiency of electrolysis.

The Cu–Cl cycle includes an energy-intensive spray drying process that can be driven by utilizing waste heat from within or external to the Cu–Cl cycle. Factoring in the additional efficiency gains realized by this waste heat recovery, it yields for System III a similar range of operational cost as the previous natural gas estimate of between $6/GJ and $7/GJ.

Note also that this approach can be adapted with the existing CANDU reactors with a top-up heat source like natural gas. This is the situation considered in System IV, introduced above. The operational cost estimate of this version of System IV is in line with the previous cost estimate, namely, at about $6.3/GJ.

The transportation costs of hydrogen from the centralized Cu–Cl plant consider truck transport at $4.6/GJ for an average distance of up to 16 km. In hydrogen transport, there lies a key synergy between off-peak electrolysis and thermochemical production of hydrogen because the trucking costs rise with distance from the Cu–Cl plant. However, decentralized electrolysis (which does not require hydrogen transportation) has lower costs further away in surrounding towns. Thus, similarly to centralized base load electricity with nuclear power, together with decentralized supply from wind or solar power, the electrolysis and thermochemical production methods have synergistic roles with each other. Similar economic trade-offs exist between thermochemical production and electrolysis with pipeline hydrogen transport as an option. Decentralized electrolysis becomes more economically attractive in towns that surround a nuclear power plant with hydrogen generation capability, because shorter pipelines are needed between fueling stations in cities.

The above systems have a unique potential to serve both decentralized needs in off-peak hours and centralized base load production from a nuclear station, respectively. This potential indicates that water-based production of hydrogen can become more competitive against the predominant existing technology provided that there is a method to effectively link these systems. A first result from the study by Naterer et al. (2008) is presented in Fig. 2.11 where the cost per GJ of hydrogen (delivered to users) for three of the systems considered in the analysis is shown: I,

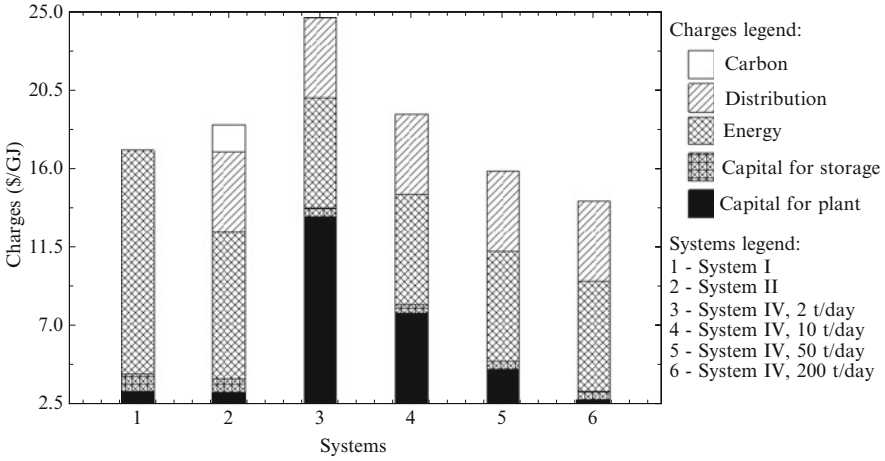

Fig. 2.11 Cost comparison of various production systems for hydrogen [data from Naterer et al. (2008)]

Table 2.1 Cost details for compared Systems I, II, and IV

			IV			
System	I (10 U × 1 t/d)	II (10 t/d)	2 t/d	10 t/d	50 t/d	200 t/d
Capital for plant ($/GJ)	3.2	3.1	13.2	7.7	4.4	2.7
Capital for storage ($/GJ)	1.0	0.8	0.5	0.5	0.5	0.5
Energy ($/GJ)	12.8	8.4	6.3	6.3	6.3	6.3
Distribution ($/GJ)	0	4.6	4.6	4.6	4.6	4.6
Carbon ($/GJ)	0	1.6	0	0	0	0
Total ($/GJ)	17.0	18.5	24.6	19.1	15.8	14.1
Total ($/kg)	2.41	2.67	3.49	2.71	2.24	2.00

II, and IV. System III is excluded in this comparative chart because the specific aim is to compare only the technology of today.

The Generation IV SCWR is still under development; therefore System III will be analyzed later with the purpose to study the potential of improvement of hydrogen production technology. The detailed structure of the cost components is indicated in Table 2.1. For capacities below ~10–20 t/day, electrolysis from off-peak electricity has a lower unit cost of hydrogen production, although the advantage reverses at higher capacities.

The next part of the study considers various scenarios of technology improvement for the Cu–Cl plant and increased benefits of hydrogen production with thermochemical cycles during off-peak periods and applications of the SCWR. Regarding technology improvement, it is assumed that in a relatively short time horizon, the capital cost of a Cu–Cl plant can be reduced by 25 %. System IV with a 25 % capital charge reduction is denoted in the next comparative graph, illustrated as Fig. 2.12, with IV-25 %. Regarding System III (SCWR), which is included in the

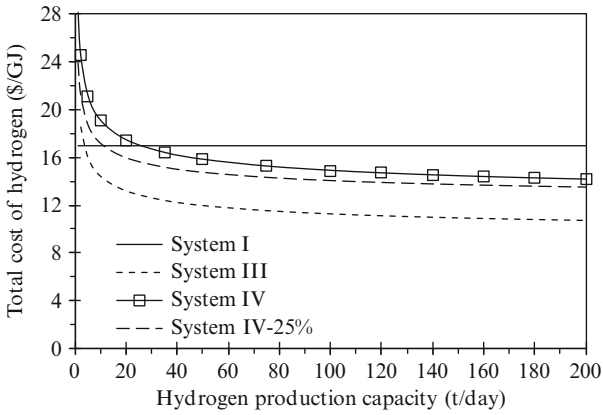

Fig. 2.12 Cost comparison of Systems I, III, III-25 %, and IV with respect to hydrogen production capacity [data from Naterer et al. (2008)]

analysis reported in Fig. 2.12, this uses the same 25 % reduced capital cost of the Cu–Cl plant.

Furthermore, System III uses off-peak times to generate more hydrogen by diverting the high-pressure/high-temperature steam from the turbine to the Cu–Cl plant using a bypass heat exchanger. During the on-peak period, the thermochemical cycle maintains a base load production of hydrogen. Discounting the energy cost by an equivalent amount as the off-peak electrolysis, a further potential cost reduction of $2.8/GJ is illustrated in Fig. 2.12 for System III. A key result is the predicted crossover point between electrolysis and thermochemical production in Fig. 2.12, at about 10–20 t/day. It should be kept in perspective that various idealizations, simplifications, and uncertainties are used in this cost analysis, so the results are intended more to provide qualitative trends, rather than precise costs.

System III appears to be the most effective with respect to Systems I and IV and IV-25 % for large-scale applications. A further discount of the hydrogen cost by System III is obtained by selling the oxygen produced from water splitting. At a market price of about $0.21/kg of oxygen, this effectively represents a discount on the hydrogen cost. In Fig. 2.13, the cost of hydrogen produced by System III if the oxygen is sold as a by-product is indicated; the system is identified on the graph with the legend "System III + oxy." This system is compared to SMR, with System II on the same chart (no carbon capture is assumed for System II). For more expanded comparisons, two systems II with CO_2 capture are considered (see Naterer et al. 2008):

- "System II + $30-carbon" using a deep geological aquifer located 300 km from the SMR plant with associated capture and sequestration costs of $30/t of CO_2.
- "System II + $100-carbon" which assumes the application of a carbon tax of $100/t of emitted CO_2.

In Fig. 2.13, it is predicted that the SMR/Cu–Cl plant crossover occurs at 70 t/day if no carbon sequestration is applied, whereas if it does apply the crossover, it

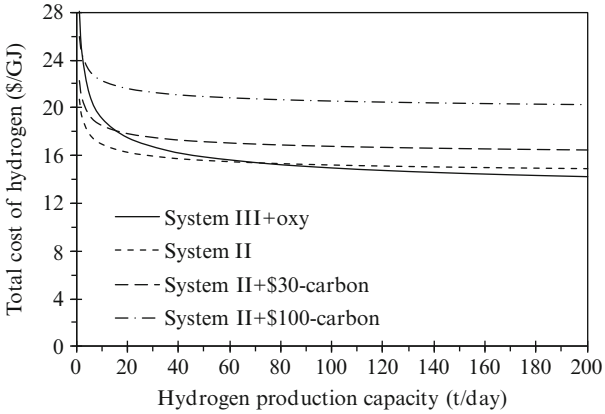

Fig. 2.13 Cost comparison between hydrogen production Systems II (SMR) and III (Cu–Cl + SCWR) for a range of production capacities [data from Naterer et al. (2008)]

occurs at about 20 t/day. Moreover, if carbon is taxed, the thermochemical production becomes competitive vs. SMR at around 5 t of hydrogen per day.

The effect of distributed nodes that leverage the synergy between decentralized hydrogen production and local community infrastructure needs can extend the production capacity of electrolyzers beyond 10 t/day of hydrogen production. Thermochemical methods have significantly higher thermal efficiency, but electrolysis can take advantage of low electricity prices during off-peak hours, local use of by-products of heat and oxygen, as well as intermittent and decentralized supplies of electricity like wind, solar, or tidal power. By effectively linking these systems, production of hydrogen from nuclear and/or renewable energy can become more competitive against SMR.

2.4 Heavy Oil Upgrading and Petrochemical Operations

The world dependence on crude oil and petroleum products will not be eliminated in the current century. The crude oil consumption in recent years increased from 11 millions of barrels per day (mbd) in 1950, to 57 mbd in 1970, to around 85 mbd at present. Crude oil (or petroleum) is a naturally occurring hydrocarbon-based liquid or solid (e.g., bitumen in oil shale, oil sands), found in underground rock formations. The main hydrocarbons included in petroleum are alkanes, cycloalkanes, aromatics, asphaltics, naphthalenes, and paraffins. From the total world crude oil reserves, 30 % is conventional oil, 15 % heavy oil, 25 % extra heavy oil and 30 % is found in forms of bitumen in oil shale and oil sands.

Historical trends of crude oil production and the forecast of future demand are indicated in Fig. 2.14. This figure has been compiled using data derived from previous studies by Dincer and Zamfirescu (2011) and Wang and Naterer (2010).

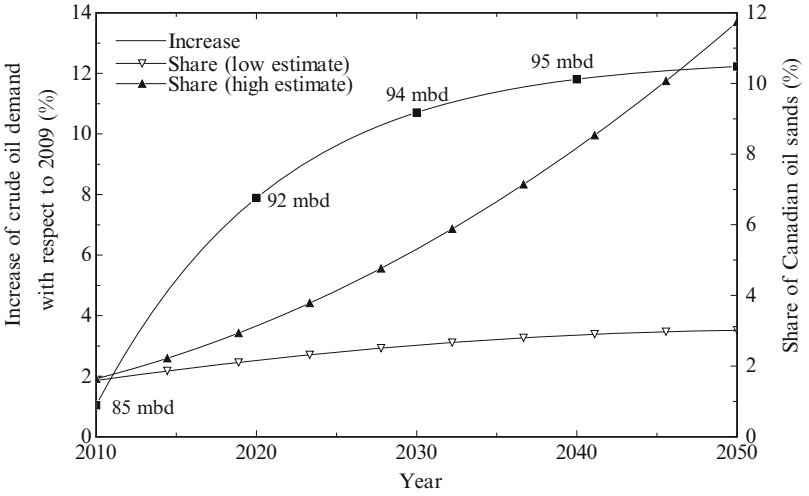

Fig. 2.14 Forecast of crude oil demand increases until 2050 and Canadian oil sands share

It is estimated that until 2040, the world crude oil demand will increase by10 % with respect to the present and afterwards will likely remain quasi-stable at around 95 mbd. Other oil reserves except conventional oil will start to be exploited in a larger degree than today. Figure 2.14 indicates the low and the high estimates of crude oil demand from Canadian oil sands. These estimates are expressed in Fig. 2.14 in percentages from the total crude oil demand of the world. By 2050, the share of Canadian oil sands—which is essentially very heavy oil—will represent between 3 and 12 % of the total crude oil demand. From this figure, one can derive that the technologies of crude oil upgrading and other petrochemical operations (distillation, extraction, fractionation, purification, cracking, etc.) must be advanced to reach higher efficiency, more cost-effectiveness, and lower pollution.

Three main commodities are mainly consumed by petrochemical refineries in order to extract and process crude oil, namely, mechanical power, heat, and hydrogen. In addition, for some processes (oil sand extraction), large quantities of water are consumed, especially in the form of steam. Mechanical power is needed to operate machines and equipment for crude oil extraction and processing. It can be found in the form of direct shaft work, electricity to operate electric motors, or a fuel (diesel, gasoline, or hydrogen in the future) to run machines. The heat is needed by many chemical processes like extraction of hydrocarbon fractions, distillation of crude oil, thermo-catalytic cracking, etc. Hydrogen is needed to upgrade crude oil to lighter fractions to fabricate diesel, gasoline, methanol, etc. With today's technology, the power, heat, and hydrogen needed in refineries and crude oil extractions from the oilfield are highly polluting with large quantities of GHGs released. Two examples of inefficient resource utilizations with today's technology include:

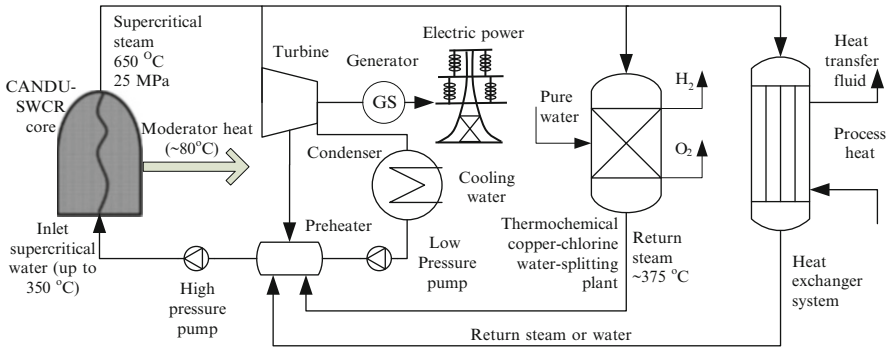

Fig. 2.15 General layout of a coupled CANDU-SWCR + Cu–Cl plant for power, heat, and hydrogen generation

- Using high-quality fuels to heat crude oil in refineries for distillation
- Using natural gas to generate hydrogen for upgrading bitumen from oil sands

This section examines the role of nuclear hydrogen generation for improving the environmental performance of heavy oil upgrading and petrochemical operations. It focuses on three major operations: extraction of bitumen from oil sands, upgrading bitumen to crude oil, and crude oil distillation to produce a range of refinery fuels. The results can be extended for oil shale extraction and upgrading without major modifications. Also, the results can be applied to refineries of traditional crude oil supplied with power, heat, and hydrogen derived from nuclear heat and water, for better cost-effectiveness and reduced pollution.

Many of the petrochemical operations require high temperatures (more than 300 °C). Therefore, the envisaged nuclear reactor is a Canadian CANDU-SCWR (Supercritical Water Reactor) of Generation IV which produces high-pressure steam at around 650 °C and 25 MPa. This steam can be used as a valuable source of power, heat, or hydrogen. Figure 2.15 presents the conceptual coupling of a CANDU-SWCR with a copper–chlorine thermochemical water splitting plant and a heat exchanger system for general-purpose petrochemical operations (including traditional oil or oil sand exploitation and bitumen upgrading). The aim of this system is to provide the required energy and material needs to petrochemical processes such that transportation fuels (gasoline, diesel, jet fuel, kerosene) and refinery by-products (fuel oil, coke, asphalt, methanol, sulfur) can be obtained without burning additional high-quality fuels, reducing thus the pollution and increasing the cost competitiveness.

In order to establish an analysis basis and compare various technologies, consider first the traditional petrochemical operations including those from oil sand extraction and upgrading—which are relatively novel developments in the oil industry. Crude oil must first be extracted from the oilfield (oil sand, oil shale field) and then it is further processed. With the current technology, there are specific materials and energy requirements for each of these two phases. The extraction work is laborious and requires costs (and energy) mainly for locating the reservoir,

drilling, oil extraction and recovery, pipelines, and truck transportation to a refinery. For the oil sands case, high energy is spent by surface mining (which is applied up to 75 m deep deposits). The deeper deposits are more economically exploited via in situ methods. Very large quantities of steam are needed to extract the bitumen from oil sands. It requires soaking, softening, bitumen slurry pumping, and separation from sand. This needs roughly 1 barrel of clean water per barrel of crude oil; for heating purposes, on average 17 cubic meters of natural gas are combusted to produce one barrel of crude oil.

Typically more than 90 % of bitumen in the oil sands is recovered while the rest of the mined material is deposited in tailing ponds which measure more than 2 m^3 for each barrel of crude oil. Fresh water must be used with the in situ extraction method (steam-assisted gravity drainage (SAGD)). A major problem is that water becomes contaminated with many pollutants including mercury, heavy metals, and naphthenic acids. In Alberta, the area covered by contaminated water in tailing ponds increased about three times in the last five years (as of 2011, it extended to around 150 km^2). The estimated GHG emission associated with oil sand extraction is 130 kg CO_2 per barrel of synthetic crude oil. The energy and GHG emissions and environmental pollution due to tailing ponds associated with oil sand exploitation are among the most significant of all oil extraction technologies.

There are some major technologies currently applied to extract bitumen from oil sands in Alberta. The most widely applied is "SAGD" which involves drilling to horizontal wells, one above and one below. Steam is injected in the above well, which soaks and softens the bitumen that flows in the bottom well. A bitumen slurry is formed, which is pumped at the surface where bitumen is separated mechanically. The process requires steam at 100–300 °C and around 17 m^3 of natural gas to be combusted. "Cyclical steam stimulation" is another method that uses only one well of steam injection and bitumen slurry extraction after soaking and softening. The "toe-to-heel air injection" method produces a combustion process in the bitumen well by injecting air; the generated heat soaks and softens the bitumen which becomes fluid and then can be extracted. "Cold heavy oil production with sand" is a method extensively applied in Alberta to unconsolidated sand stones; the method uses sand to enhance the bitumen extraction. The SAGD method is also applied with other working fluids than steam. One version is to use hydrocarbon solvents to dilute and slightly upgrade the bitumen; this method is called "vapor extraction."

Another promising version is to use supercritical carbon dioxide ($ScCO_2$). It is shown by Fang (2010) that the optimum pressure and temperature of supercritical carbon dioxide extraction for oil sands are ~25 MPa and 60 °C. This creates a large potential to use low-grade heat recovery. Moreover, the bitumen separation process is very much facilitated by an application of pressure swing principles and recycling of carbon dioxide. After the mechanical separation of bitumen from sand and other impurities at optimal pressure and temperature, a further separation is required: separation of bitumen from carbon dioxide. Pressure swing separation implies a sharp reduction of pressure to 7 MPa (slightly below the critical pressure). Thus, carbon dioxide transforms in the gas phase and what remains is a hot liquid bitumen

Table 2.2 Required inputs for selected petrochemical processes for 1 barrel of crude oil

Process		Inputs
Bitumen extraction from oil sands[a]	SAGD	Steam at 100–300 °C; 27 m^3 natural gas as heat for 1 barrel of crude
	$ScCO_2$	CO_2 at 25 MPa, 60 °C
Bitumen upgrading to crude oil		Hydrogen
Crude oil distillation		2 kg steam at 2 bar 400 °C for 1 barrel of crude oil 102 MJ of heat at 400 °C for 1 barrel of crude oil

[a]Includes oil sand extraction from the well

Table 2.3 Bitumen upgrading temperatures and process description

Upgraded oil type	*T* (°C)	Brief process description
Athabasca bitumen	350–530	Thermal cracking, fluidized bed
Canada bitumen	380–460	Hydrothermal visbreaking, in supercritical water
Fort McMurray (Alberta) oil sands	400	Natural zeolite cracking
Heavy oil	450–550	Treated zeolite catalytic cracking
Alberta bitumen	500	Delayed coking
Alberta bitumen	300–400	Hydro-treating
Heavy oil	450	API 618 standards upgrading
Alberta bitumen	525	Hydrocracking
Canada bitumen	300–400	Fixed bed, removal of S, N, and O
Canada bitumen	410–420	Single cracker, increase H/C ratio
Canada bitumen	470–510	Fluid catalytic cracker

at low pressure. The captured carbon dioxide is recompressed to around 8 MPa, condensed at ~30 °C, repressurized to 25 MPa, heated, and reinjected in the well. In contrast, with $ScCO_2$ extraction in SAGD, water cannot be reinjected due to contaminants. Moreover, the contaminated steam cannot be released into the atmosphere. Therefore, with SAGD, steam is condensed and the resulted contaminated water is accumulated in tailing ponds, as also mentioned above.

Table 2.2 lists the input requirements for a bitumen extraction process, and two other petrochemical processes: bitumen upgrading to crude oil and crude oil distillation. The data from Table 2.2 is derived from the studies of Wang et al. (2010), Dincer and Rosen (2007), and Fang (2010). Regarding bitumen upgrading to crude oil, the required temperatures and process parameters are listed in Table 2.3. In Alberta, most of the hydrogen is produced in SMR plants along Edmonton's "Upgrader Alley." The temperature required by the upgrading depends strongly on the bitumen properties, cracker type, processing method, and upgrading degree, which can be synthetic crude oil or lighter oil, depending on the amount of hydrogen addition.

The crude oil distillation requires steam and heat in the approximate amounts listed in Table 2.2 for 1 barrel of crude oil. By distillation, a large pallet of refinery fuels is obtained: wash oil, heavy gas oil, light gas oil, heavy-to-light diesel, kerosene, naphtha, and liquefied petroleum gas (LPG). Steam is needed in the

Table 2.4 GHG emissions of bitumen extraction from Canadian oil sands using gas for heating

Year	2015	2020	2025	2030
Bitumen production scale (10^6 barrels/day)	2.2	3.4	4.1	4.3
Natural gas volume for heating (10^6 m^3/day)	59.5	90.6	110.4	116.1
Heat supplied by natural gas (MW_{th})	25,603	39,379	47,487	49,803
GHG emissions from combustion for heat (10^6 t/year)	42.6	65.6	79.1	83.0
Compared with 2006 CO_2 emissions (% of 2006)	7.8 %	12.0 %	14.5 %	15.2 %

Note: Canada's total CO_2 emissions in 2006 were 544.68×10^6 t

process of distillation; some 5 % of the supplied steam is recovered as water. As indicated in Dincer and Rosen (2007), the overall efficiency of double-stage distillation plants is around 55 %. A part of the fuel products are combusted to generate flue gas at 1,100 °C for heating.

In the situation, when a system sketched in Fig. 2.15 is used to provide power, heat, and hydrogen to the operations (extraction, upgrading, distillation, etc.) there are no direct GHG emissions. For a comparative analysis purpose, various common methods can be considered to supply these petrochemical processes with heat, power, and hydrogen. For instance, heat can be supplied by combustion of natural gas or by electric heating. In both cases, there are associated GHG emissions if the electricity is derived from the local grid. In Alberta and Saskatchewan—where oil sands are exploited—84 and 60 % of the power generated to the grid, respectively, are due to fossil fuel combustion.

Assume an evolution of Canada's production of oil sand bitumen according to Table 2.4, which falls in the range predicted in Fig. 2.10 (discussed above). It is possible to calculate the GHG emissions due to natural gas combustion for bitumen extraction. Natural gas is used for methane, in which one generates 1 mol of CO_2 per combusted mole of fuel. If bitumen extraction continues to be driven by natural gas combustion, the associated GHG emissions by 2030 would represent a large 15.2 % portion of total CO_2 emissions of Canada in 2006.

Regarding hydrogen production, the traditional methods that compete with the solution proposed in Fig. 2.15 (CANDU SWCR + Cu–Cl cycle) are SMR, coal gasification, and water electrolysis using electricity from the grid. Other alternative methods include the use of the copper–chlorine cycle to split water. The energy to drive the Cu–Cl process can be derived from natural gas combustion or nuclear heat. Each case will be considered.

SMR proceeds with syngas production followed by a water gas shift reaction. It consumes more methane than the stoichiometric balance to compensate for the need of reaction heat; this heat is obtained by combustion of additional methane. For full conversion, the overall reaction is $1.315CH_4 + 1.37H_2O + 0.63O_2 = 1.315CO_2 + 4H_2$. In practice, the yield of hydrogen is 65 % on average; therefore one obtains

$$\text{Emissions (SMR)} = 0.51CO_2/H_2(\text{combustion of methane as the heat source}). \tag{2.4}$$

However, if the heat needed to supply SMR is derived from a clean source such as solar energy (required 800 °C), then no direct GHG emissions are associated with it. Therefore, the net GHG emission of SMR becomes

$$\text{Emissions (SMR)} = 0.39\text{CO}_2/\text{H}_2(\text{clean heat source},\ T > 800\,^\circ\text{C}). \tag{2.5}$$

Coal gasification occurs at 800–1,800 °C according to the endothermic reaction $2H_2O + C = CO_2 + 2H_2$. If heat is supplied to the reaction by combustion of additional coal, the stoichiometric equation becomes $2H_2O + 1.453C + 0.453O_2 = 2H_2 + 1.453CO_2$. The practical conversion efficiency of coal to hydrogen is 60 % and the thermal efficiency of the process is assumed to be around 70 %. Therefore,

$$\text{Emissions (coal gasification)} = 1.21\text{CO}_2/\text{H}_2(\text{combustion of coal as the heat source}) \tag{2.6}$$

and

$$\text{Emissions (coal gasification)} = 0.84\text{CO}_2/\text{H}_2(\text{clean heat source},\ T > 800 - 1,800\,^\circ\text{C}). \tag{2.7}$$

The GHG emissions of water electrolysis are correlated with the emissions of electricity generation. In order to make comparisons with SMR and coal gasification on a common basis, assume, conservatively, that electricity is generated from natural gas with 30 % efficiency, and water is dissociated through electrolysis with 100 % efficiency. This process occurs according to the following overall reaction: $1.187(CH_4 + 2O_2) + H_2O = 1.187(CO_2 + 2H_2O) + H_2 + 0.5O_2$. Therefore,

$$\text{Emissions (water electrolysis, 100 \% fossil fuel power)} = 1.19\text{CO}_2/\text{H}_2. \tag{2.8}$$

For Alberta and Saskatchewan, the emission equations—considering 84 and 60 %, respectively—for GHG emissions due to combustion of fossil fuels in power generation (see above) and assuming that natural gas is mainly used in these provinces for power generation yield

$$\left.\begin{array}{c}\text{Emissions (electrolysis, 84 \% fossil fuel power, Alberta)} = 0.99\text{CO}_2/\text{H}_2 \\ \text{Emissions (electrolysis, 60 \% fossil fuel power)} = 0.72\text{CO}_2/\text{H}_2\end{array}\right\}. \tag{2.9}$$

Note that the emissions of water electrolysis appear higher than SMR. To lower them to the SMR level, the clean power fraction of the grid must be in excess of 70 %. Next, consider hydrogen production with the Cu–Cl cycle when the heat needed to sustain its reaction is derived from natural gas combustion.

To produce one mole of hydrogen, the total required heat by all endothermic reactions is 555 kJ and the total released heat of all exothermic processes is 232 kJ within the Cu–Cl cycle. Assume that 50, 70, 80, and 90 % of the heat released by exothermic processes in the Cu–Cl cycle is recycled internally within the cycle. Then the required high-temperature heat input is 220 MJ/kg, 197 MJ/kg, 185 MJ/kg, and 173 MJ/kg H_2, respectively. Assume that there are no heat losses from the combustion chamber and that natural gas can be modeled as methane. All of the combustion heat of natural gas is transferred to the cycle. Therefore, the overall chemical equation to split water using the Cu–Cl cycle with heat from the combustion of methane is

$$x \times (CH_4 + 2O_2) + H_2O = x \times (CO_2 + 2H_2O) + H_2 + 0.5O_2, \tag{2.10}$$

where x is the molar fraction of methane that must be added to the cycle to make itself sustainable.

The values for x are 0.548, 0.489, 0.460, and 0.432 when the released heat is 50 %, 70 %, 80 %, and 90 % reused internally, respectively. Because methane burning generates steam, this can be used in the Cu–Cl cycle as a portion of feed H_2O; the other portion will be liquid water that must be boiled. Together with steam, CO_2 is introduced into a hydrolysis reaction of the Cu–Cl process, hence a need for separating HCl from CO_2 in the downstream units. However, the introduction of CO_2 also has significant advantages: (a) heat carried in high-temperature CO_2 of the methane combustion exhaust gases can be recovered back to the hydrolysis reaction; and (b) CO_2 is inert to $CuCl_2$ and can reduce the decomposition of copper oxychloride. Therefore, if steam and carbon dioxide are recycled to provide part of the heat (and feed) to the Cu–Cl plant, then the molar fraction x from (2.10) becomes 0.47, 0.42, 0.40, and 0.37, when the released heat by exothermic processes of the Cu–Cl cycle is 50, 70, 80, and 90 % reused internally.

The Cu–Cl cycle requires electricity to drive the electrolytic process of CuCl/HCl aqueous system. Assume that this electricity is derived from the local grid (for Alberta and Saskatchewan cases). Therefore, the corresponding GHG emissions are

$$\left.\begin{array}{c}\text{Emissions (electrolysis Cu}-\text{Cl, 84 \% fossil fuel power, Alberta)} = 0.07CO_2/H_2 \\ \text{Emissions (electrolysis Cu}-\text{Cl, 60 \% fossil fuel power)} = 0.05CO_2/H_2\end{array}\right\}. \tag{2.11}$$

The results regarding GHG emissions per mole of hydrogen produced with all considered methods are summarized in Tables 2.5 and 2.6. Table 2.5 shows those methods that use a fossil fuel heat source. Table 2.6 indicates the hydrogen production methods with anon-carbon heat supply. In both cases, the required electricity is supplied from the local grid. It is found that the Cu–Cl cycle has the lowest CO_2 emissions.

When fossil fuels are used as an electricity and heating supply to the Cu–Cl cycle, then the cycle has equivalent or slightly lower emissions than SMR,

Table 2.5 GHG emissions of H_2 production using fossil fuel heat source with various methods

Method	GHG[a]	Description of the system
SMR	0.51	The burning of methane supplies all of the required enthalpy of endothermic processes.
Coal gasification	1.21	The burning of coal supplies all of the required enthalpy of endothermic processes.
Water electrolysis	1.19	100 % of the electricity is supplied from the combustion of fossil fuels.
	0.99	84 % of the electricity is supplied from the combustion of fossil fuels (AB).
	0.72	60 % of the electricity is supplied from the combustion of fossil fuels (SK).
Cu-Cl cycle	0.44 (AB) 0.42 (SSK)	90 % The burning of methane supplies all of the net heat input to the Cu–Cl cycle. The electricity for the electrolytic step of Cu–Cl cycle is supplied from the power grid: Alberta, 84 % fossil fuel generated; Saskatchewan, 60 % fossil fuel generated. The percentages are the internally reused portions of the heat released by exothermic processes of the Cu–Cl cycle after the steam in the exhaust gases produced from the methane combustion is recovered.
	0.46 (AB) 0.44 (SK)	80 %
	0.48 (AB) 0.46 (SK)	70 %

[a]Given in mol CO_2 emitted per mole H_2 produced

Table 2.6 GHG emissions of H_2 production using non-carbon heat supply with various methods

Method	GHG[a]	Description of the system
SMR	0.39	The enthalpy of endothermic processes is completely supplied from clean heat sources.
Coal gasification	0.84	The enthalpy of endothermic processes is completely supplied from clean heat sources.
Cu–Cl cycle	0.07 (AB) 0.05 (SK)	The net heat input to the Cu–Cl cycle is completely supplied from non-carbon heat sources, e.g., solar or nuclear, but the electricity for the electrolytic step of the Cu–Cl cycle is supplied from the power grid: Alberta, 84 % fossil fuel generated; Saskatchewan, 60 % fossil fuel generated.
	0	If the electricity for the electrolytic step of the Cu–Cl cycle is completely clean from a non-carbon source (SWCR + Cu–Cl system).

[a]Given in mol CO_2 emitted per mole H_2 produced

depending on the steam and heat recovery percentages. When non-carbon heat sources are used, the level of CO_2 emissions of SMR is about eight times higher than the Cu–Cl cycle. If both heat and electricity supplies are clean, then SMR still has significant emissions while the Cu–Cl cycle produces none.

With the current SMR technology used to generate hydrogen for bitumen upgrading of Canadian oil sands, the GHG emissions increase in the near future according to the forecast shown in Table 2.7. It will reach around 10 % of Canadian CO_2 emissions in 2006. These emissions come on top of emissions due to bitumen

Table 2.7 GHG emissions of hydrogen production for bitumen upgrading with SMR technology

Year	2015	2020	2025	2030
Bitumen production scale (10^6 barrels/day)	2.2	3.4	4.1	4.3
Hydrogen for upgrading (t/day)	7,480	11,560	13,940	14,620
GHG emissions from SMR process (10^6 t/year)	30.0	46.4	56.0	58.7
Compared with 2006 CO_2 emissions (% of 2006)	5.5 %	8.5 %	10.3 %	10.8 %
Heat supplied by SWCR to produce H_2 ($MW_{thermal}$)[a]	19,046	29,435	35,495	37,227
Number of SCWR + Cu–Cl plants required[b]	1.4	2.2	2.7	2.8

Note: Canada's total CO_2 emissions in 2006 were 544.68×10^6 t

[a]Hydrogen is produced by CANDU-SWCR and Cu–Cl plant linkage according to system from Fig. 2.15

[b]Assumed six nuclear reactors per plant, for equivalent 1,000 $MW_{electric}$ each unit

Data from Wang and Naterer (2010)

Table 2.8 GHG emissions of oil sand extraction, upgrading, and distillation with current technology (SAGR, SMR, and natural gas combustion at refinery)

Year	2015	2020	2025	2030
GHG emissions for bitumen extraction (10^6 t/year)	42.6	65.6	79.1	83.0
GHG emissions from SMR process (10^6 t/year)	30.0	46.4	56.0	58.7
GHG for crude oil distillation (10^6 t/year)	10.0	15.2	18.2	19.2
Total GHG emissions (10^6 t/year)	82.6	127.2	153.3	160.9
Compared with 2006 CO_2 emissions (% of 2006)	15 %	23 %	28 %	30 %

Note: Canada's total CO_2 emissions in 2006 were 544.68×10^6 t

extraction via SAGD (see Table 2.4). By 2030, the total emissions for bitumen extraction and upgrading to crude oil are predicted to represent 25 % of total Canadian CO_2 emissions in 2006. Herein lies a benefit of using nuclear hydrogen production with CANDU-SWCR and the Cu–Cl cycle (Fig. 2.15). Based on the amount of required hydrogen, the number of nuclear plants to be installed in the oil sand locations is indicated in Table 2.7. If such an investment is pursued, the GHG emissions remain at the level of 15 % with respect to the year 2006, corresponding to the bitumen extraction process, only.

For distillation of one barrel of crude oil, one needs 2 kg of steam at 2 bar and 400 °C, and 102 MJ of heat (see Table 2.2) with 55 % efficiency. Assume that the heat to generate steam is derived from natural gas combustion; moreover, the heat needed to drive the distillation process is derived also from natural gas combustion (this scenario models today's refinery technology). It results in roughly 200 MJ of natural gas that must be combusted to satisfy these heating needs. Therefore, 4.2 kg of methane must be combusted to distillate 1 barrel of crude oil. The corresponding GHG emissions are12 kg CO_2 per distilled barrel of crude oil. The total carbon emissions with current technology are shown in Table 2.8. From Table 2.8, by applying SWCR and Cu–Cl technology, at least 30 % of GHGs are mitigated for oil sand extraction, upgrading, and distillation. This can be achieved by installing three nuclear plants.

For the year 2030, the GHG mitigation in terms of tons of CO_2 equivalent of Canadian oil sand processing is presented in Fig. 2.16. It can be observed that the

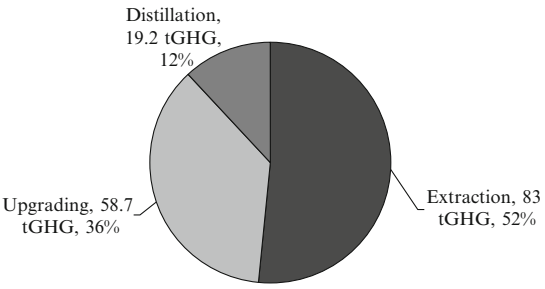

Fig. 2.16 GHG mitigation by 2030 if nuclear hydrogen with CANDU SCWR and Cu–Cl water splitting cycle is applied to Canadian oil sand processing

majority of GHG mitigation is due to improving the extraction process, whereas the heat needed to drive the process is replaced with carbon-free nuclear heat. Upgrading of bitumen is the second major segment of environmental improvement, achievable by providing heat and hydrogen from nuclear reactor energy. The distillation of crude oil in a refinery accounts for 12 % mitigation of GHG emissions.

Thus, by using nuclear hydrogen, in conjunction with nuclear heat and power in the petrochemical sector—more specifically oil sand processing—major GHG pollution reductions can be achieved. Additional gains of environmental performance are achieved by improving the extraction technology for bitumen. Application of $ScCO_2$ extraction—currently in development—reduces the water and energy requirements, as well as creates the opportunity to sequester CO_2 in situ, at oil sand locations.

2.5 Nuclear-Produced Hydrogen for the Transportation Sector

2.5.1 Transportation Sector Outlook

The transportation sector is characterized by intense energy demand in any country. Taking Canada as a sample case, Fig. 2.17 indicates the distribution of energy demand and GHG emissions for the transportation sector of this country. In Canada, the transportation sector accounts for about 32 % energy demand and 35 % GHG emissions. It can be observed that road transport is responsible for 78 % of GHG emissions in this sector.

Figure 2.18 shows the fuel consumption in the Canadian transportation sector, as per fuel type. Motor gasoline is the major fuel in Canada; its consumption represents 54 % in energy terms from all fuels. Diesel fuel follows gasoline with 33 %, and next is aviation fuel with 10 %. Figure 2.19 details the energy and GHG emissions for all kinds of transport vehicles in Canada. According to this data, the most pollution is due to passenger cars (25.3 %) and heavy trucks (23.3 %). It is expected that in the near future the global demand for transportation of goods and people will significantly increase. If the transportation demand increases at the same pace with global population, the level of pollution rises significantly. In this section, the role of nuclear hydrogen for a cleaner and better transportation sector is studied.

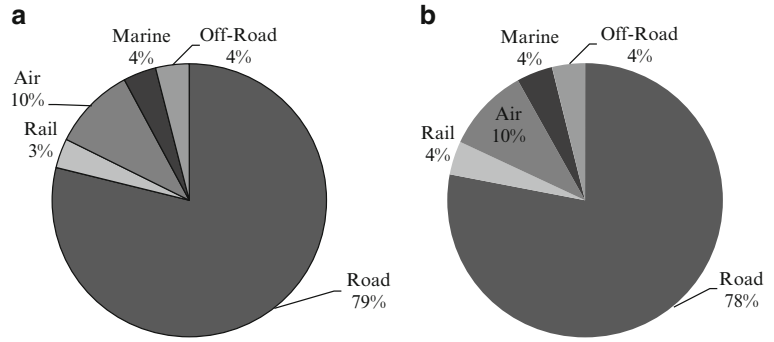

Fig. 2.17 Energy (**a**) and GHG emissions (**b**) by the transportation sector of Canada for each major transportation mode in 2008 [data from NRCAN (2010)]

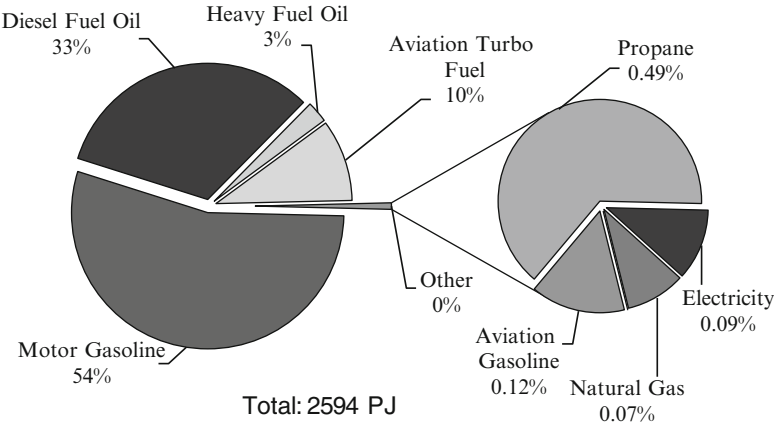

Fig. 2.18 Fuel consumption in Canadian transportation sectors, per fuel type [data from NRCAN (2010)]

Hydrogen is a potential energy carrier for powering all kinds of vehicles for road, rail, marine, air, and space transport. In Sect. 2.3 it is shown how hydrogen—as an energy carrier—can be generated using the power grid and base load nuclear energy with positive consequences on the electricity price, pollution reduction due to better operation of the grid, and additional pollution reduction due to promotion of hydrogen as an energy carrier for fuel cell vehicles.

2.5.2 Hydrogen-Fuelled Road Transport

The general layout of a fuel cell vehicle and hydrogen supply side is outlined in Fig. 2.20. Hydrogen is generated at partly centralized locations at the site of nuclear

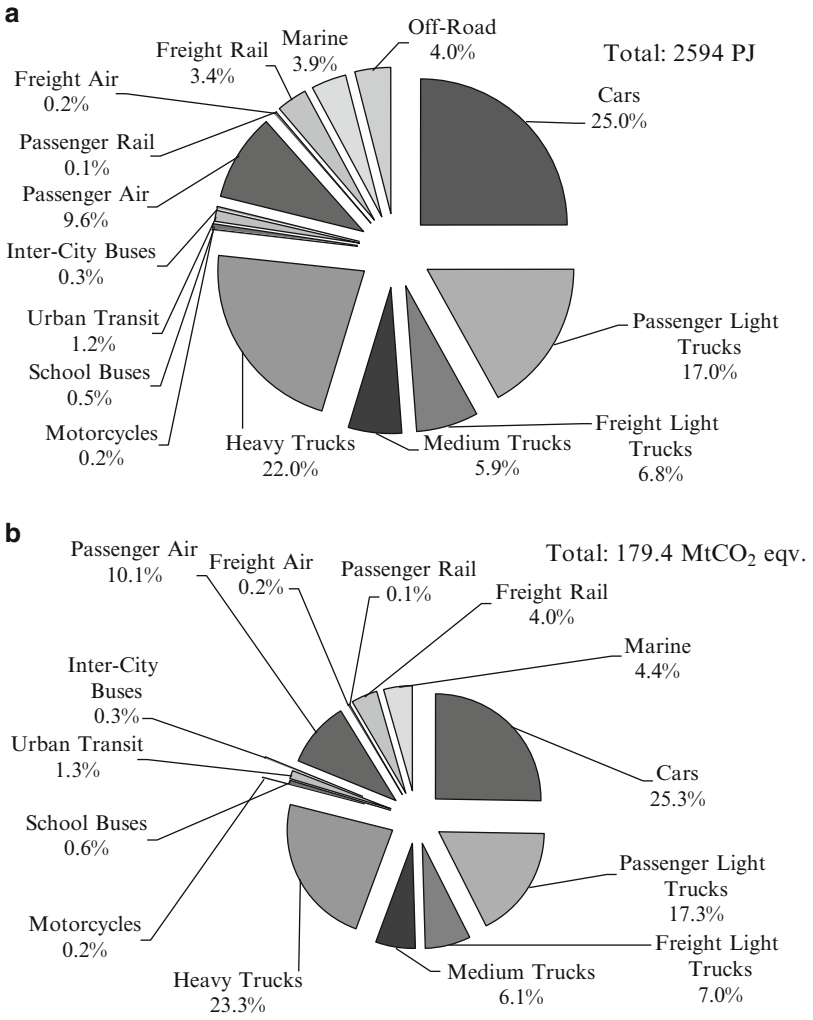

Fig. 2.19 Energy consumption (**a**) and GHG emissions (**b**) of transportation vehicles in Canada as per 2008 (*source*: NRCAN 2010)

power plants, and partly generated at decentralized locations using grid electricity and electrolysis. The energy utilization in the overall system from Fig. 2.20 (including fuel cell vehicles and the hydrogen supply system) can be estimated based on past studies; Dincer et al. (2010) and Dincer and Zamfirescu (2011). Figure 2.21 indicates the energy utilization in fuel cell cars.

Note that the results reported in Fig. 2.21 are estimates and refer only to typical fuel cell cars. Most of the losses are from hydrogen production and supply and due to hydrogen conversion back to electricity (overall totalling 65 %). In fuel cell cars, the shaft work for propulsion represents around 24 % of the primary energy. Using

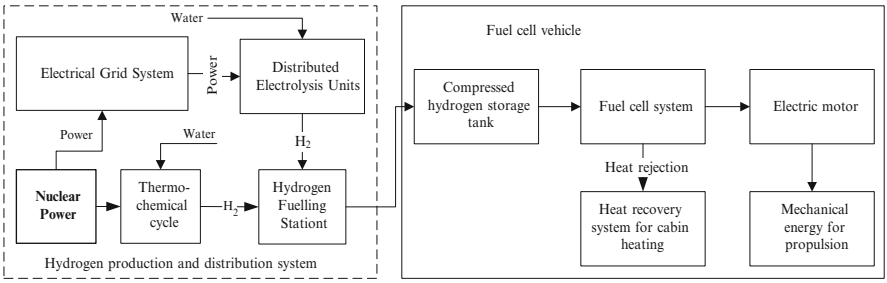

Fig. 2.20 Main subsystems of a fuel cell vehicle and hydrogen supply

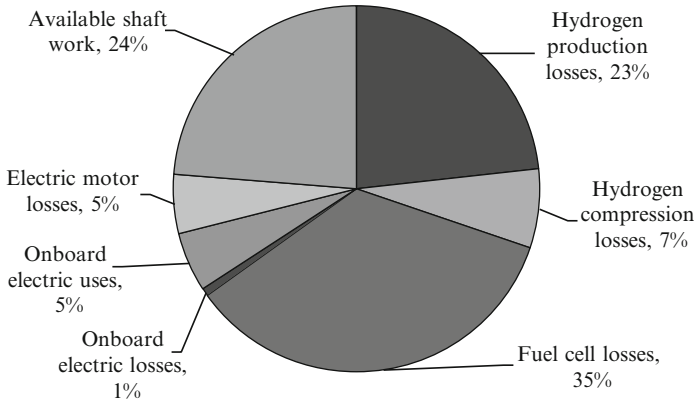

Fig. 2.21 Energy utilization in a typical fuel cell vehicle with respect to primary energy

actual electrical grid data from Environment Canada (2010), estimates are made based on energy utilization of fuel cell vehicles (Fig. 2.21) for the GHG emissions of electricity-driven passenger cars for each province. For comparison purposes, two types of electricity-driven cars are considered, namely, the fuel cell vehicle and electric vehicle. It is assumed that the vehicles are supplied by the electricity grid.

For the electric vehicle, it is assumed, based on data from Dincer et al. (2010), that there is a 54 % electricity to shaft power efficiency. The results presented in Fig. 2.22 show that the application of electric vehicles in Canada is beneficial except in three provinces where electrical grids are characterized by high GHG pollution due to their fossil fuel-based power sources. Future grid improvements by (potentially) adding nuclear-hydrogen capacity in Alberta, Saskatchewan, New Brunswick, and Nova Scotia can foster growth of fuel cell vehicles together with electric vehicles in all Canadian provinces. Fuel cell vehicles have a longer driving range than electric vehicles, which also cannot be used reliably yet in severe climatic conditions when cabin heating or cooling is needed, because in such cases, the driving range of electric vehicles may become significantly reduced in many situations.

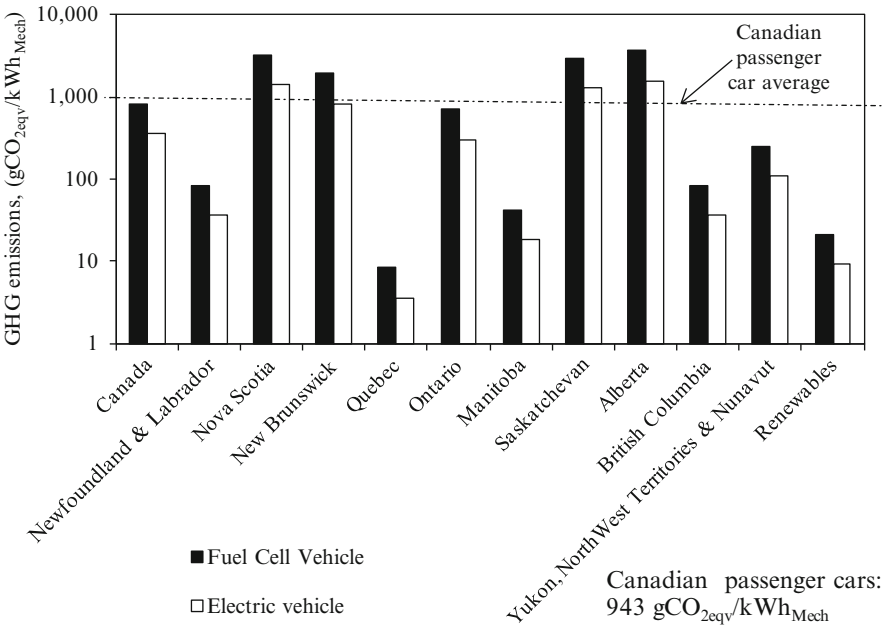

Fig. 2.22 Estimates of GHG emissions of electricity-driven passenger cars in Canada

Apart from electric and fuel cell vehicles, the hybrid powertrains appear as a promising solution for sustainable transportation. Figure 2.23 compares the GHG emissions and air pollution indicators for hybrid, electric, fuel cell, and conventional passenger cars. The air pollution indicator quantifies the environmental impact of exhaust gases of automobiles other than GHGs, which include the following airborne pollutants: CO, NO_x, SO_x, and volatile organic compounds (VOCs). According to Dincer et al. (2010), the indicator uses the following weighting coefficients: 0.017, 1, 1.3, and 0.64, for each airborne pollutant, respectively.

In the study reported in Fig. 2.23, four real vehicles are considered: Toyota Corolla (conventional), Toyota Prius (hybrid), Toyota RAV4EV (electric), and Honda FCX (fuel cell). It is assumed that hydrogen is generated by grid electricity assuming average worldwide pollution indicators associated with electricity generation; these indicators are taken from the study of Dincer et al. (2010), namely, 77.5 g GHGs per MJ of electricity and 0.296 g/MJ as the air pollution indicator. All three alternative vehicle options reduce the life cycle pollution to about half, with respect to a conventional vehicle. However, fuel cell vehicles show the smallest air pollution among all, during the vehicle utilization stage. The electric vehicle is characterized by air pollution during the utilization stage due to its battery recycling, mainly. If the GHGs of hydrogen production decrease, the fuel cell vehicle has the best likelihood to have the lowest carbon footprint.

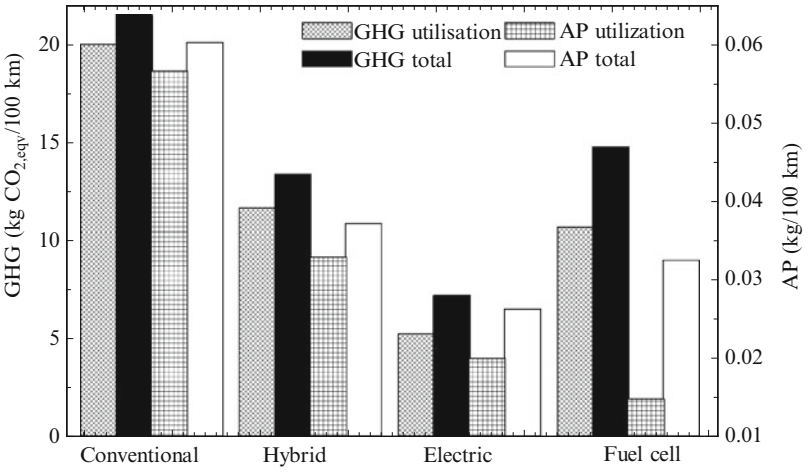

Fig. 2.23 GHG and air pollution (AP) related to the fuel utilization stages and total environmental impact for different types of vehicles [data from Dincer et al. (2010)]

2.5.3 Hydrogen-Fuelled Railway Transport

For large-scale transportation (trains, ships, airplanes), it appears feasible to store hydrogen onboard in its pure form. One of the first applications of hydrogen for widespread transportation vehicles may be implemented at a large scale in the near future for train locomotives, which offer an attractive mode of transportation in terms of energy consumption per passenger kilometer of travel. An option for cleaner rail transport is electrification with an electricity supply from clean generators (such as hydro, nuclear, wind, etc.). Electrified trains transfer more than 85 % of the electricity input to the wheels, making it one of the most efficient transportation systems, when compared with private automobiles, buses, or airplanes. Disadvantages of electrification include the capital investment to install electrical substations and catenaries, together with a lack of flexibility for locomotives to move into other service areas not covered by electrification. In two papers by Marin et al. (2010a, b), a case study of hydrogen train implementation in Ontario is presented for the 115 km "GO Transit Lakeshore" corridor, through Toronto, between Oshawa and Hamilton, Ontario, which currently carries a total of approximately 100,000 passengers each weekday. The Lakeshore corridor operates locomotives on diesel fuel at a rate of approximately 5 L/km pulling/pushing 10 or 12 carriages with up to 1,540 passengers during peak hours.

Passenger use projections for this corridor are expected to grow by about 90 % for Lakeshore East and 65 % for Lakeshore West between 2007 and 2031, respectively. A sensitivity analysis was performed over a range of operational costs for a hydrogen train, with variability of feedstock prices, fuel cell power density, and expected return on capital investment. According to general estimates (see Marin et al. 2010a), the initial capital cost for train electrification in 2007 was in the order of 5.9 billion

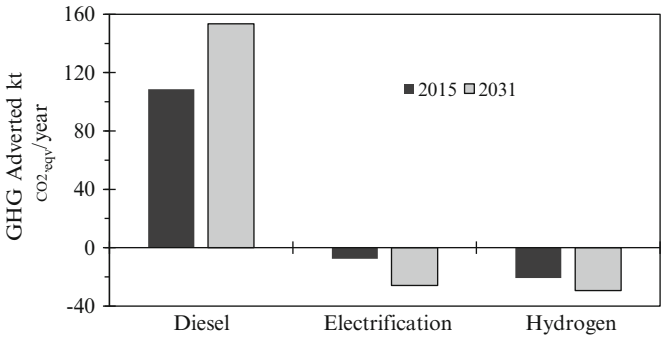

Fig. 2.24 Total equivalent GHGs averted by train transport [data from Marin et al. (2010a)]

Canadian dollars. The operation of the electrified corridor varied between 78 and 145 $/train-km, projected to 2015, while hydrogen operation had a cost varying between 79 and 151$/train-km, with a capital cost varying from 12.5 to 16 %.

The estimated power at the prime mover is on the order of 0.09 GJ/km. This figure offers a basis for modeling of fuel cell trains with an added benefit of higher fuel efficiency between 53 and 58 %. One drawback of fuel cell trains is the required refurbishing at approximately 5,000 h of operation, much less when compared to a diesel engine that requires a complete overhaul every 15,000–25,000 h of operation, although continual advances are being made to improve fuel cell durability.

Figure 2.24 provides a comparison of averted emissions based on different power sources, against distance travelled by trains annually. On the basis of the source energy, whether nuclear, Ontario Power Generation (OPG) mix in Ontario, Canada, or hydrogen from SMR, the utilization of heat rejected from thermal powerplants, combined with hydrogen generated through a thermochemical Cu–Cl cycle and proton exchange membrane fuel cell (PEMFC) trains, results in the lowest level of GHG emissions, on the order of 0.10 kg/GJ.

The higher efficiency of the PEMFC complements the performance of thermochemical hydrogen production, yielding the lowest GHG emissions at the prime mover, on the order of 0.04 kg/km (345 t by 2015, and 488 t by 2031). The actual impact of CO_2 emission reduction is significant when compared to the diesel alternative. Further GHG emission forecasts from GO trains—depending on the propulsion option—are indicated in Fig. 2.25.

When comparing the electrification to hydrogen train alternatives, it is assumed that capital expenditures for infrastructure not related to hydrogen remain unchanged. The cost per kilogram of hydrogen is the combined result of several factors, including the capital cost of building the hydrogen plant, the cost of operating and maintaining the plant, the cost of feedstock (whether it is gas, electricity, or thermal energy), the cost of capital invested, the cost of compression and storage, the cost of transportation and delivery, and other miscellaneous external costs not listed here, all included in this analysis. The economic parameters used to generate the results—for the case study of implementation of hydrogen trains in Ontario—are listed in Table 2.9.

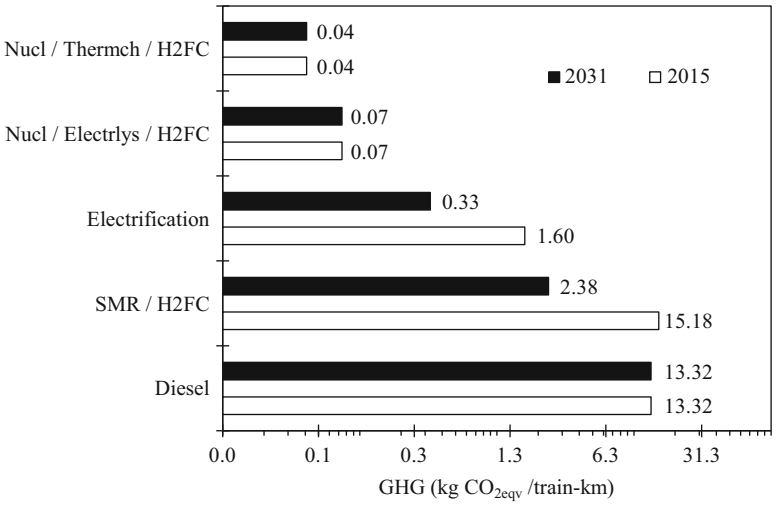

Fig. 2.25 Total GHG emissions from GO trains predicted between 2015 and 2031 [data from Marin et al. (2010a)]

The energy requirement for locomotive propulsion is given by the following equations for thermochemical hydrogen production, electrolysis, and electrification, respectively:

$$\left.\begin{aligned} E_{\text{th}} &= \frac{E_{\text{pm}}}{\eta_{\text{fc}}\,\eta_{\text{c}}\,\eta_{\text{th}}} \\ E_{\text{e}} &= \frac{E_{\text{pm}}}{\eta_{\text{fc}}\,\eta_{\text{c}}\,\eta_{\text{e}}\,\eta_{\text{pp}}} \\ E_{\text{el}} &= \frac{E_{\text{pm}}}{\eta_{\text{t}}\,\eta_{\text{pp}}} \end{aligned}\right\}, \tag{2.12}$$

where E is energy, η is efficiency, and the subscripts signify thermochemical (th), electrolysis (e), electric train (el), prime mover (pm), fuel cell (fc), compression (c), turbine conversion of electrical power (pp), and transmission and distribution of electric power (t).

The results of cost modeling are indicated in Fig. 2.26, showing the cost contributors to the production of hydrogen as a percentage of total cost. The feedstock cost, capital cost, and transportation costs are included. Transportation of hydrogen is typically in the range of 0.3–1.3$/kg. It is compared at operational costs for annual payment of compound interest and capital at the rate of 12.5–16 %, with natural gas costs varying from 5 to 9$/GJ.

The analysis from Fig. 2.27 assumes electricity costs to vary from 32 to 100$/MWh; and thermal power costs vary from 9 to 11.6$/GJ. Figure 2.26 illustrates the capital cost estimates for hydrogen trains, with consideration given to the most probable scenario of fuel cell cost, at the time of introduction into the market. The costs of capital and electricity influence significantly the operational cost of trains when hydrogen is generated via electrolysis. Figure 2.28 shows the expected range

Table 2.9 Economic parameters considered for hydrogen train modeling

Parameter	Equation	Description
Annual payment of compound interest	$A = C \times (1+i)^n \times \frac{i}{(1+i)^n - 1}$	Determines the contribution of capital cost to the cost of hydrogen. It is applied to the construction phase and long-term capital financing of a project
Capital cost contribution	$\mathrm{Hc} = \frac{A}{\mathrm{Dy} \times 24 \times \mathrm{Rh}}$	Represents the contribution of capital costs to hydrogen product cost
Present value of investment	$C = \frac{\mathrm{Ck}}{(\mathrm{Ac}/\mathrm{Nc})^f}$	Predicts the cost of a scalable chemical plant as a function of known capital cost (Ck)
Cost of hydrogen transportation	$\mathrm{Ht} = \mathrm{const} \times \mathrm{Dp}^{1.0146}$, where $\mathrm{const} = 0.0027 - 0.0031$	Represents the contribution of hydrogen transportation towards the cost of hydrogen product via pipeline

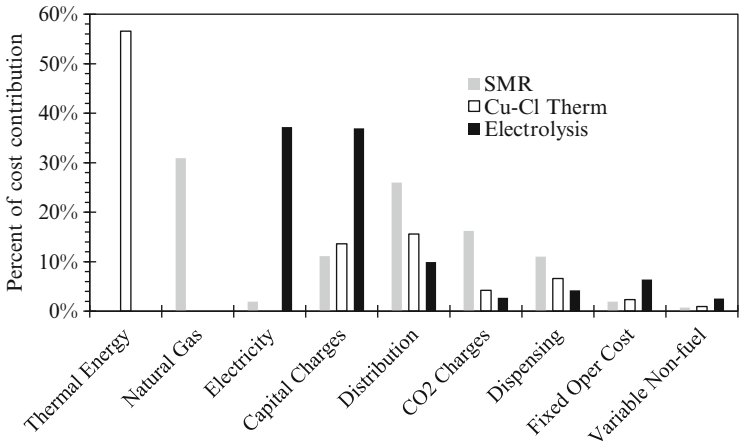

Fig. 2.26 Cost contributors to the production of hydrogen as a percent of total cost [data from Marin et al. (2010a)]

of trains versus onboard hydrogen storage. Under the assumption that GO trains stay at stations an average of 14 % of total traveling time, a 5 % minimum safe hydrogen mass remaining in storage before refuelling, and fuel cell efficiencies at 50 %, the expected range with an initial hydrogen storage of 1,800 kg is approximately 1,000 km.

Another important aspect which influences the economics of either electrification or "hydrogenenation" of GO Lakeshore trains is represented by transportation of the energy carrier from its production source to the locomotive. In the case of electrification, it is necessary to transport the electricity from remote power plants, which may involve up to 9 % transmission losses. These losses are seen as a proportional increase of electricity price (as delivered to the locomotive). Pipeline transportation of hydrogen at high volumes can be as low as \$0.1/kg, while liquid hydrogen transportation reaches \$0.3/kg. From an economics perspective, the investment required to provide power substations and catenaries for electrification is contrasted

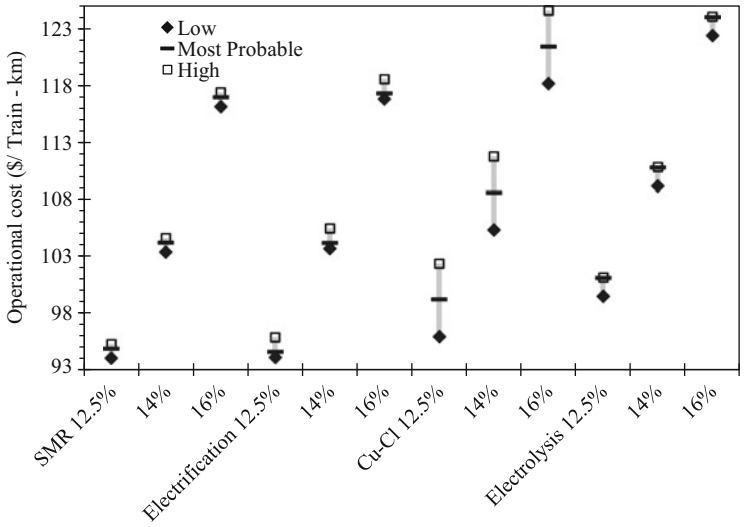

Fig. 2.27 Range of total operational cost of GO train Lakeshore Corridor, based on variable feedstock costs and equal annual payments at 12.5, 14, and 16 % compound interest on capital [data from Marin et al. (2010a)]

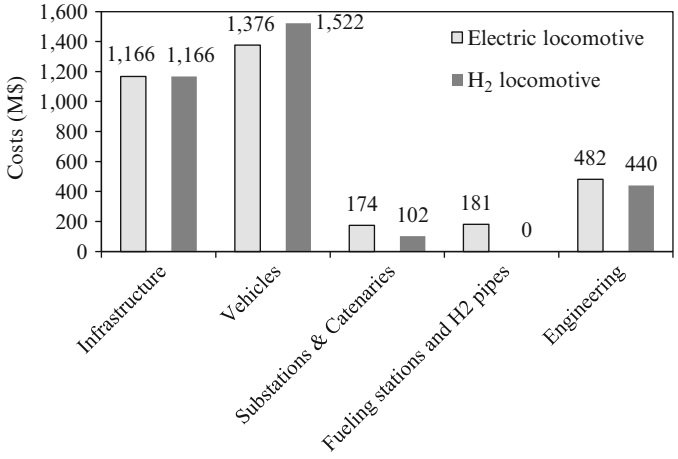

Fig. 2.28 Comparative cost of capital investments via electrification vs. hydrogen fuel cell locomotives [data from Marin et al. (2010a)]

with the investment in refuelling stations and hydrogen delivery via piping, respectively. Electrical transformer substations in the case of electrification have a cost impact that can be compared to filling stations in the case of hydrogen fuel.

Based on the above results, it appears that the GO hydrogen train is promising with major environmental advantages, but also drawbacks such as high cost and relatively short lifetime of PEMFCs. It was found in Marin et al. (2010b) that

scaled-up fuel cells can fit within the existing Bombardier ALP-46A locomotives, including hydrogen gas storage. The electrification of train operations in the Lakeshore corridor may also be affected by CO_2 legislation in direct proportion to the electricity mix established by OPG. Since this energy mix is projected to contain a portion based on fossil fuels, there is some uncertainty in the potential increase in the cost of operation per train-km. This uncertainty contrasts with the uncertainty of fuel cell prices in the future. While the cost associated with GHG emissions will inevitably increase in the future, the cost of fuel cells is projected to be lower as the technology develops, matures, and reaches mass production.

2.5.4 Hydrogen-Fuelled Airway Transport

Hydrogen is also a promising alternative for future aircraft fuel because of its high energy content per unit of mass and favorable combustion kinetics, reduced environmental impact, and increased sustainability. The environmental impact of liquid hydrogen fuel with respect to the reference kerosene jet fuel is compared in a study by Nojoumi et al. (2009). According to past Airbus research, for 3.3 m^3 of LH_2 and a wind speed of 4 m/s in the case of an accidental crash, an area of about 1,000 m^2 of fire carpet would arise, in comparison to 13,500 m^2 for propane. In this respect, LH_2 is a safer aviation fuel than kerosene.

During the flight, airplanes form condensation trails that represent artificially induced cirrus clouds. The tank of a proposed hydrogen aircraft can be placed above the payload, above and aft of the payload, or fore and aft of the payload section. The fore tank can be located between the cockpit and forward passenger compartment bulkhead, and the aft tank is located between the aft passenger compartment bulkhead and tail area. The tanks can either be integral or nonintegral parts of the fuselage structure. Storing LH_2 instead of kerosene by volume has a ratio of 4:1. An additional heat exchanger is needed with respect to a kerosene fuelling configuration to heat the liquid hydrogen to a temperature that is suitable for injection into the combustion chamber.

As derived from the combustion equation, $C_{12}H_{23} + 17.75O_2 + 66.77\ N_2O_2 \rightarrow 12CO_2 + 11.5H_2O + 66.77N_2$ for complete stoichiometric combustion of 1 kg of kerosene; 3.4 kg of oxygen is needed, producing 3.16 kg of CO_2, 1.24 kg of water vapor, 1 g of NO_x, and between 1 and 2.5 g of CO. A typical passenger airplane consumes for a trip from Toronto to Calgary about 13,937 kg of kerosene (for a distance of 2,716 km). Table 2.10 shows detailed emission analysis of flight, landing, and takeoff for the Airbus A300 airplane at selected destinations departing from Toronto.

A liquid hydrogen (LH_2) aircraft has quieter operation with respect to conventional aircraft due to a smaller engine, which has a more compact cooling system with liquid hydrogen rather than air. The engine life is increased by about 25 % and maintenance requirements are also reduced. Figure 2.29 compares volumetric specific fuel consumption of an Airbus A300 when operated with conventional fuel or cryogenic hydrogen.

Table 2.10 Total emissions for Airbus A300 airplane at selected destinations from Toronto

City	Montreal	Calgary	London
Distance (km)	504	2716	5710
Fuel consumption (kg)	3,677.3	13,937.3	19,005
Climb/cruise/descent (kg)	2,875	13,751.4	17,553.7
Specific consumption (kg/km)	7.29	5.13	5.55
NO_x (kg) total	56.17	171.4	251.7
Climb/cruise/descent	45.29	171.5	214.0
HC (kg) total	2.43	4.19	5.10
Climb/cruise/descent	0.5	2.30	3.03
CO (kg) total	21.9	32.2	39.2
Climb/cruise/descent	3.1	10.25	12.74
GHG emissions (kg $CO_{2,eqv}$)	22.34	15.71	19.85

Data from Nojoumi et al. (2009)
HC hydrocarbon emissions, *CO* carbon monoxide emissions, NO_x nitrogen oxide emissions

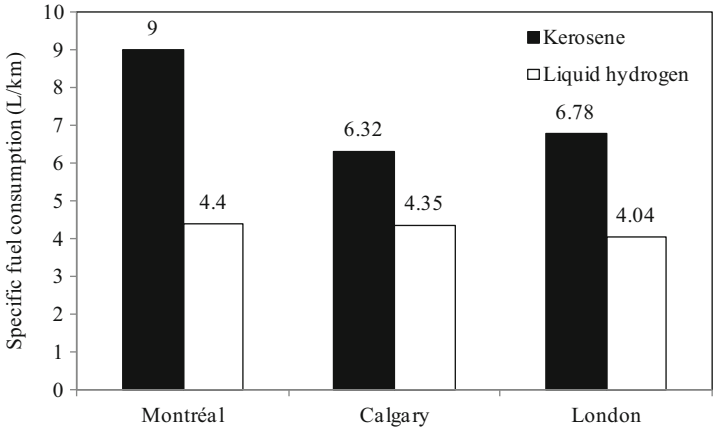

Fig. 2.29 Specific fuel consumption for conventional and hydrogen Airbus A300 departing from Toronto towards three destinations [data from Nojoumi et al. (2009)]

2.5.5 Hydrogen Role for Reducing Environmental Impact in Transportation Sector

If hydrogen is used as fuel in transportation sector, the associated GHG emissions and global warming effect can be fully mitigated. GHGs emitted are inevitable with fossil fuel-propelled transportation vehicles that are majorly in use today, but in hydrogen vehicles there are zero GHGs emitted and therefore no effect on global warming potential (excluding the emissions from the process of generating hydrogen).

The concentration of GHGs in the atmosphere influences the radiative balance on earth. The *radiative forcing* (denoted with ΔF) represents the net change in radiation balance at the tropopause level, produced by a specified cause. It induces an increase of planet temperature when the radiative forcing is positive. Typically

the radiative forcing is smaller than 2 W/m^2. The global mean concentration of CO_2 in the atmosphere in 2005 was 379 ppm, leading to a ΔF of +1.66 [±0.17] W/m^2.

The NO_x emissions from transportation vehicles of all kinds tend to increase the ozone level. As an example, for supersonic aircraft at high altitudes above 18 km, ozone is depleted in large extend. An increase in the concentration of ozone in the upper troposphere is more effective in increasing ΔF than lower altitude. Therefore, LH_2 aircraft should be used at lower altitudes below 12 km. Other emissions from a hydrogen airplane is water vapor, but their effect on radiative forcing is minimal because their lifetime in the troposphere is short (around 10 days), and typically removed with precipitation. Condensation trails produced from high-altitude aircraft exhaust cause radiative forcing and thus they may affect climate. They can persist for many hours, depending on their condition and local weather patterns, reflect solar radiation, and absorb and emit thermal infrared radiation. Aviation in general has the potential to change cirrus clouds in a number of ways. Contrails do not always evaporate after a short time. If the local atmosphere is supersaturated with respect to ice, the clouds will form into larger cirrus clouds called contrail cirrus, which cannot be distinguished from contrails, if the concentration is unknown.

The radiative forcing is calculated by using the formula recommended by Intergovernmental Panel on Climate Change (IPCC):

$$\Delta F = 6.3 \times \ln (C/C_0), \tag{2.13}$$

where C_0 is the concentration of carbon dioxide at a reference time, which typically is taken as 280 ppm, corresponding to the beginning of the industrial era; C is the change in carbon dioxide concentration.

With this formula, the radiative forcing can be calculated for specific means of transportation based on an initial concentration of carbon dioxide in the atmosphere. The total mass of the atmosphere is about 5×10^8 kg with an average temperature of 15 °C; therefore a volume estimated with the ideal gas law is 9.2×10^{14} m^3. The mass of carbon dioxide at the beginning of the industrial era is estimated based on C_0 and it is about 920 Gt. Using the data from the Canadian transportation sector which emits in total 180 Mt GHG per annum, the radiative forcing can be determined when produced if this sector is supplied with nonpolluting energy. The result is -12.3 mW/m^2 for a decade. Figure 2.30 presents this analysis for four transportation means in Canada: car, heavy truck, train, and ship. On the same plot, the specific GHG emissions are shown per MJ of energy consumed by the transportation sector. The statistical data from NRCAN (2010), regarding GHG emissions and fuel consumption, are used in this analysis (see Fig. 2.19). It can be observed that vehicles generate the smallest quantity of GHGs while rail transport generates the highest.

Note that the radiative forcing influences global warming through the so-called climate sensitivity factor defined by

$$\gamma = \frac{\Delta T_e}{\Delta F}, \tag{2.14}$$

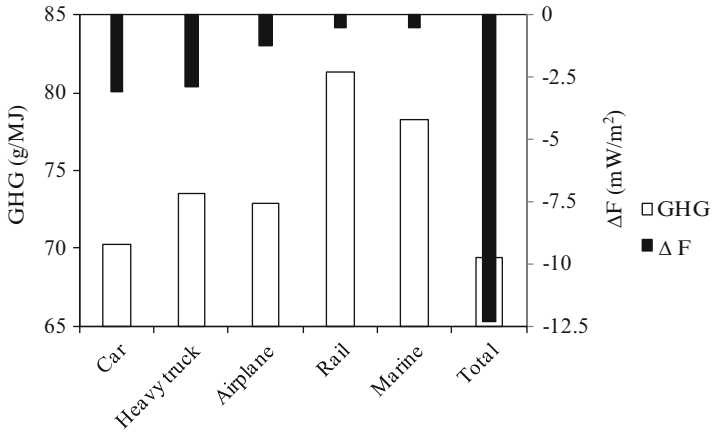

Fig. 2.30 Specific GHG emissions by means of transportation in Canada and the radiative forcing due to GHG mitigation in this sector

where ΔT_e represents the increase of earth's temperature due to the radiative forcing ΔF. The current estimated value of the climate sensitivity factor is 0.6 m^2K/W (see Dincer and Zamfirescu 2011). With a total anthropogenic radiative forcing of 61 mW/m^2 per decade, it shows that the temperature increase within 10 years may be about 0.04 °C. Using an average of -10 mW/m^2 for the radiative forcing created by GHG gases from the entire Canadian transportation sector, it yields a result wherein the total radiative forcing may decrease to 51 mV/m^2; therefore the increase of the earth's temperature may reduce to 0.03 °C.

2.6 Conclusions

In this chapter, the role of nuclear energy in hydrogen production has been examined. It was shown that hydrogen is important for better environmental performance, efficiency, and cost effectiveness in various industrial and other sectors. The roles of hydrogen in three sectors are studied in more detail, namely, electricity generation and distribution, petrochemical operations, and the transportation sector. These sectors are significant in the future hydrogen economy. Nuclear power offers a base load capability and all other power generators operate at fluctuating loads as a function of demand and fuel availability. Operation at part load is not optimal and leads to more fuel consumption and more GHG emissions for the same output (power generation).

The role of nuclear power is crucial in the future for a base load source of power generation without GHG emissions. Generation IV nuclear power plants (e.g., SWCR-CANDU) can be coupled with thermochemical cycles (such as the Cu–Cl cycle) to generate hydrogen at base load conditions. Nuclear hydrogen production can operate in synergy with water electrolysis at delocalized stations which operate

intensely during off-peak periods. During the peak periods, hydrogen can be converted back to electricity with fuel cells. When it is advantageous, hydrogen can be sold as a fuel to the transportation sector, or feedstock in various chemical and other industries. Load levelling for the grid through nuclear hydrogen is a useful outcome with better matching between supply and demand.

Another major application is hydrogen use for upgrading of oil sands in petrochemical operations. Both conventional oil and oil sands are envisaged as high future consumers of hydrogen. Nuclear energy can provide heat, power, and hydrogen as outputs for processing of fossil fuels (including extraction, upgrading, distillation, and hydro-treating).

Hydrogen is often cited to become a major fuel for the transportation sector worldwide in the future. It is important that hydrogen is generated from clean sources to reduce GHG pollution and the global warming effect. Various scenarios of hydrogen vehicle implementation in society were analyzed in this chapter. Hydrogen can be readily used for vehicles although further developments are required for fuelling and storage systems, fuel cells, and infrastructure. Sustainable hydrogen production is an essential requirement and it will have a crucial role in facilitating the future hydrogen economy.

Nomenclature

C Cost, any currency
E Energy (MJ)
F Radiative forcing (W/m^2)
G Gibbs free energy (MJ/kg)
H Reaction enthalpy (kJ)
$\dot{m}$ Rate of hydrogen production (t/day)
Q Heat flux (kJ)
S Reaction entropy (kJ/kg K)
T Temperature (K)
x Molar fraction of methane

Greek Letters

γ Climate sensitivity factor
η Efficiency

Subscripts

0 Reference value
c Compression

ΔG	Gibbs free energy
e	Electrolysis or earth
el	Electric power train
fc	Fuel cell
pm	Prime mover
pp	Turbine conversion of electrical power
ref	Reference
SMR	Steam methane reforming
t	Transmission and distribution of electric power
tot	Total
th	Thermochemical, thermal
$T\Delta S$	Heat transfer irreversibilities
w	Per unit of energy

References

Carty RH, Mazumder MM, Schreiber JD, Pangborn JB (1981) Thermo-chemical hydrogen production. Final report IGT Project 30517, Institute of Gas Technology, USA

Dincer I, Rosen MA (2007) Exergy: energy environment and sustainable development. Elsevier, Boston, MA

Dincer I, Rosen MA, Zamfirescu C (2010) Economic and environmental comparison of conventional, hybrid, electric and hydrogen fuel cell vehicles. In: Pistoia G (ed) Electric and hybrid vehicles: power sources, models, sustainability, infrastructure and market. Elsevier, Amsterdam

Dincer I, Zamfirescu C (2011) Sustainable energy systems and applications. Springer, New York

Environment Canada (2010) Electricity intensity tables. http://www.ec.gc.ca/ges-ghg/default.asp?lang=En&n=EAF0E96A-1

Fang Y (2010) Extraction of hydrocarbons from oil sand using supercritical carbon dioxide. MSc thesis, University of Alberta

IESO (2011) Monthly market report: July 2011. Independent Electricity System Operator. www.ieso.ca. Accessed 16 Aug 2011

Marin G, Naterer GF, Gabriel KS (2010a) Rail transportation by hydrogen vs. electrification—case study for Ontario Canada, I: propulsion and storage. Int J Hydrogen Energy 35:6084–6096

Marin G, Naterer GF, Gabriel KS (2010b) Rail transportation by hydrogen vs. electrification—case study for Ontario Canada, II: energy supply and distribution. Int J Hydrogen Energy 35:6097–6107

Naterer GF, Fowler M, Cotton J, Gabriel K (2008) Synergistic roles of off-peak electrolysis and thermochemical production of hydrogen from nuclear energy in Canada. Int J Hydrogen Energy 33:6849–6857

Nojoumi H, Dincer I, Naterer GF (2009) Greenhouse gas emissions assessment of hydrogen and kerosene fueled aircraft propulsion. Int J Hydrogen Energy 34:1363–1369

NRCAN (2010) National energy use database. Natural resources of Canada. http://oee.nrcan.gc.ca/corporate/statistics/neud/dpa/data_e/databases.cfm?attr=0

Orhan MF (2011) Conceptual design, analysis and optimization of nuclear-based hydrogen production via copper-chlorine thermochemical cycles. PhD thesis, University of Ontario Institute of Technology

Wang Z, Naterer GF (2010) Greenhouse gas reduction of oil sands upgrading and extraction operations with thermochemical hydrogen production. Int J Hydrogen Energy 35:11816–11828
Wang Z, Naterer GF, Gabriel K (2010) Clean hydrogen for oil sands upgrading with CANDU and SCWR nuclear reactors. Second Canada-China joint conference on supercritical water-cooled reactors, Toronto, ON, 25–28 April

http://www.springer.com/978-1-4471-4937-8

Hydrogen Production from Nuclear Energy

Naterer, G.F.; Dincer, I.; Zamfirescu, C.

2013, XIV, 492 p., Hardcover
ISBN: 978-1-4471-4937-8